Workplace exposure to nanoparticles during thermal spraying of ceramic coatings

Salmatonidis A.[1,2]*, Ribalta C.[1,2], Sanfélix V.[3], Bezantakos S.[5], Biskos G.[6], Vulpoi A.[4], Simion S.[4], Monfort E.[3], Viana M.[1]

[1]Institute of Environmental Assessment and Water Research (IDAEA-CSIC),08034 Barcelona, Spain

[2]University of Barcelona, Faculty of Chemistry, 08028 Barcelona, Spain

[3]Institute of Ceramic Technology (ITC), Universitat Jaume I, 12006 Castellón, Spain

[4]Institute of Interdisciplinary Research in Bio-Nano-Sciences (ICI-BNS), Babeș-Bolyai University, 400000 Cluj-Napoca, Romania

[5]Université du Littoral Côte d'Opale, 59140 Dunkerque, France

[6]Energy Environment and Water Research Centre, The Cyprus Institute, 2121 Nicosia, Cyprus

*Author to whom correspondence should be addressed. e-mail: apostolos.salmatonidis@idaea.csic.es

Abstract

Thermal spraying is widely used for industrial-scale application of ceramic coatings onto metallic surfaces. The particular process has implications for occupational health, as the high energy process generates high emissions of metal-bearing nanoparticles. Emissions and their impact on exposure were characterised during thermal spraying in a work environment, by monitoring size-resolved number and mass concentrations, lung-deposited surface area, particle morphology and chemical composition. Along with exposure quantification, the modal analysis of the emissions assisted in distinguishing particles from different sources, while an inhalation model provided evidence regarding the potential deposition of particulate matter on human respiratory system. High particle number (>10^6/cm^3; 30-40 nm) and mass (60-600 μgPM_1/m^3) concentrations were recorded inside the spraying booths, which impacted exposure in the worker area (10^4-10^5/cm^3, 40-65 nm; 44-87 μgPM_1/m^3). Irregularly-shaped, metal-containing particles (Ni, Cr, W) were sampled from the worker area, as single particles and aggregates (5-200 nm). Energy dispersive X-ray analysis confirmed the presence of particles originated from the coating material,

establishing a direct link between the spraying activity and exposure. In particle number count, 90% of the particles were between 26-90 nm. Inhaled dose rates, calculated from the exposure levels, resulted in particle number rates ($\dot{n}$) between 353×10^6-1024×10^6/min, with 70% of deposition occurring in the alveolar region. The effectiveness of personal protective equipment (FPP3 masks) was tested under real working conditions. The proper sealing of the spraying booths was identified as a key element for exposure reduction. This study provides high time-resolved aerosol data which may be valuable for validating indoor aerosol models applied to risk assessment.

Keywords: nanoparticles; exposure assessment; inhalation exposure; inhalation model; occupational health; modal analysis; process-generated nanoparticles

Introduction

In numerous industrial sectors such as petroleum (Moskowitz 1993), naval (Baiamonte et al 2015), automobile (Gérard 2006), or aeronautical and space (Pawlowski 2008a, Strangman 1985), metal structures and mechanical parts are exposed to highly corrosive environments, and subject to mechanical and chemical abrasion. In these cases, protective ceramic coatings are widely used to prevent corrosion and wear, as well as to restore damaged surfaces (Lima and Marple 2006, Tan et al 1999, Toma et al 2010). Such coatings are frequently applied using thermal spraying techniques, where the feedstock (the coating material) is projected at high temperature and velocity onto the surface to be protected or repaired. Different types of spraying torches (electric arc, plasma, flame) define the types of thermal spraying techniques (Pawlowski 2008b).

This industrial process has been reported to generate high concentrations of nanoparticles (NP, with diameters < 100 nm) at pilot-plant scale (Viana et al 2017), which may result in occupational hazards (Hériaud-Kraemer et al 2003). Previous studies of thermal spraying emissions using offline measurements focused on the chemical characterisation of particles collected on filters

(Huang et al 2016, Petsas et al 2007), showing also that these sources are associated with high particle mass concentrations. Furthermore, high NP number concentrations (> $10^9/cm^3$) were monitored directly from electric arc guns (Bémer et al 2010). At pilot-plant scale, Viana et al. (2017) showed that NP released during atmospheric plasma spraying may impact worker exposure significantly. Despite the widespread industrial application of thermal spraying, emissions generated under real-world operating conditions are not well studied. Similarly to thermal spraying, the emissions of NP from other industrial processes and their impact on worker exposure is a growing topic of research (Ding et al 2017, Fonseca et al 2015, 2016, 2018, Fujitani et al 2008, Koivisto et al 2018, Koponen et al 2015, Kuhlbusch et al 2004, Losert et al 2014, Salmatonidis et al 2018, Viitanen et al 2017), and requires further investigations due to the large variety of processes and exposure scenarios. Awareness for nanomaterial release was raised (Maynard et al 2006, Poland et al 2008, Seaton et al 2010) since the use of manufactured nanomaterials (MNMs) in workplaces started. However, NP emissions can arise from multiple processes that neither produce nor use nanomaterials, which are referred as Process Generated Nanoparticles (PGNP) (Van Broekhuizen, et al 2012).

Pope et al (1995) associated air pollution with adverse health effects based on epidemiological evidence. Further epidemiological and toxicological studies showed that $PM_{2.5}$ (particles with diameter ≤2.5 μm) is a health hazardous pollutant (Gakidou et al 2017, Landrigan et al 2017, C Pope et al 2002, C. Pope and Dockery 2006, WHO 2017). More specifically, aerosol particles <100 nm (ultrafine) are linked to adverse health effects mainly due to exposure through inhalation (Araujo et al 2008, Hoek et al 2010, Ibald-Mulli et al 2002, Knibbs et al 2011, Landrigan et al 2017, Oberdörster 2001). In indoor air and more specifically in industrial settings, PGNPs pose an occupational risk, since they are unintentionally generated and released to the worker area, and they are potential health hazards (Koivisto et al., 2014). Health risks need to be dealt with by

means of both technological and non-technological mitigation strategies (Ganser and Hewett 2017, Hallé et al 2015, Hewett and Ganser 2017, Shaffer and Rengasamy 2009).

The aim of this work was to assess NP emissions during thermal spraying of ceramic coatings onto metallic surfaces and their impact on inhalation exposure, under actual operating conditions in a real-world industrial setting. A near field (NF) / far field (FF) approach as used by Koivisto et al.(2015), among others, was applied. Workplace exposure monitoring strategies applied followed good practice as described by Asbach et al. (2015) and Brouwer et al. (2014), which were the base for internationally-recognised standard procedures (OECD.82, 2017). Modal analysis based on time-resolved particle number concentrations was used to quantitatively understand the size distribution and modal dependence of the aerosols generated during thermal spraying (Hussein et al 2005). Finally, a case study testing the effectiveness of mitigation strategies is presented.

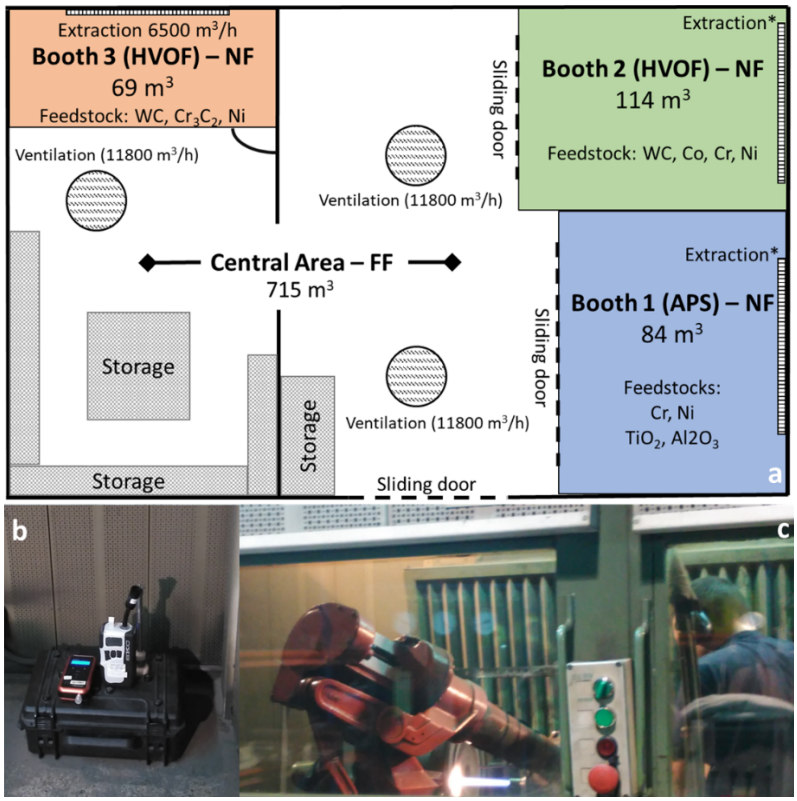

Figure 1. (a): Schematic representation of the thermal spraying section of the investigated facility (Extraction*: data not available). (b): instrument deployment in the near field location. (c): booth #3, showing the thermal spraying robot and the operator processing one of the work-pieces.

Methods and Materials

Work environment

Monitoring of thermal spraying was carried out at an industrial-scale precision engineering workshop (T.M. Comas) located in the vicinity of Barcelona, Spain. Measurements were carried out over a 5-day period in April 2017, and did not interfere with the usual operating conditions in the plant. The thermal spraying facilities are schematically depicted in Figure 1 (top). Three thermal spraying booths were located in an area of approximately 240 m^2 (14 m wide and 17 m in length), including also a storage and a central corridor. In all cases the operators of the thermal spraying equipment worked inside and outside the booths during spraying, and each booth had doors which were not always closed. Two small-scale sand blasting boxes for polishing the final pieces were located next to the spraying booths, but they were not operated simultaneously to the activities reported in this work. A general ventilation system operated constantly in the central area, with three extractors having a flow of 11800 m^3/h each (data provided by the company, not measured directly in this work). Additionally, in each of the plasma booths individual localised extraction systems were available (Figure 1a, Table 1). Information regarding the individual extraction air flowrates was only available for booth #3 (6500 m^3/h). The operational characteristics of each of the spraying activities and booths are summarised in Table 1. Because the duration of the individual spraying activities varied according to the parts to be coated, mean values of spraying duration and repetitions were different for each booth (Table 1).

Thermal spraying techniques and feedstock

Two different types of thermal spraying techniques were assessed:

- Atmospheric Plasma Spraying (APS), characterised by high temperatures (5000-20000 ºC) and projection velocities of 200-500 m/s. This technique was applied in plasma booth #1 (Figure 1). APS is generally used to project oxides and metals, which in this case of our measurements were a TiO_2-Al_2O_3 blend and a Cr-Ni blend (2 different feedstock materials that were applied separately).
- High Velocity Oxy-Fuel coating spraying (HVOF), characterised by high velocities (425-1500 m/s) and lower temperatures (2900 ºC). This type of spraying was applied in booths #2 and #3 (Figure 1b, bottom). Due to the lower temperatures compared to APS, HVOF is frequently used to project carbides and metals. During our measurements a WC-Co-Cr-Ni blend feedstock was used in booth #2, and a WC-CrC-Ni blend in booth #3.

Additional information about the feedstock powders is provided in Table S1 (Supplementary Data).

Particle monitoring and sampling

Particle number concentration (N), size-segregated mass concentrations (PM_x), size distribution, mean diameter (D_p) and lung-deposited surface area (LDSA) were monitored at near field (NF) and far field (FF) locations. The NF location was inside each of the spraying booths, while the FF was next to the storage area in the case of booth #3 and in the middle of the central area in the case of booths #2 and #3 (Figure 1a). The monitoring instruments in the FF and their inlets were located between 0.7 and 1.5 m above ground and were not placed directly inside the breathing zone (Ojima, 2012). The resulting measurements were considered representative of worker exposure, by assuming that the concentrations in the NF and FF were well-mixed. The online particle monitors deployed were:

- A Miniature diffusion size classifier “DiSCmini” (TESTO AG), that can measure particles having sizes from 10 to 700 nm, and can report total particle number (N), mean particle diameter (D_p) and lung deposited surface area (LDSA) with a 10 s time resolution. This instrument was deployed both in the NF and FF locations.
- A Mini Laser Aerosol Spectrometer “Mini-LAS 11-R” (GRIMM), that was used to measure particles in the size range 0.25-32 µm, and report total and size-segregated particle mass concentrations in 31 channels with a 6 s time resolution. This instrument was deployed both in the NF and FF locations.
- An Electrical mobility spectrometer “Nanoscan-SMPS” (TSI model 3910), covering particles in the size range 10-420 nm, that was used to measure the particle mobility size distributions in 13 channels with a 1-min time resolution. This instrument was deployed only in the FF location.
- A Mini Wide Range Aerosol Spectrometer “Mini-WRAS” (GRIMM), that can measure particles having sizes from 10 nm to 35 µm, for monitoring the particle mass concentrations across 41 channels. This instrument was also deployed in the FF location.

The mini-LAS units were operated enclosed in a protective case with a vertical stainless steel inlet (Figure 1b). Inlet extension tubes were not used for any of the other instruments. The default (manufacturer) impactor was used for the DiSCmini (cut-off diameter of 700 nm) and the default cyclone (cut-off diameter of 550 nm) was used for the Nanoscan. The DiscMini and MiniWRAS instruments were inter-compared prior to the measurements at an air quality monitoring station in Barcelona (Spain), using ambient air aerosols. The comparison resulted in R^2 coefficients >0.89, and as result the instruments were considered comparable for the purpose of our study (Table S2).

In addition to the online measurements described above, samples were collected on electron microscopy grids (Agar scientific Quantifoil 200 Mesh Au) for offline morphological and

physicochemical particle characterisation. A Leland pump (SKC Inc.) with a flow of 5 L/min was connected to a cassette (SKC inlet diameter 1/8 inch and filter support pads that were 25 mm in diameter) to which the microscopy grid was attached. The morphology and primary particle size of the particles collected were analysed using Transmission Electron Microscopy (TEM; Jeol, JEM 1220, Tokyo, Japan) and TEM/HRTEM, FEI, Tecnai F20 (200 KV, Eindhoven, Netherlands) coupled with an Energy-Dispersive X-ray (EDX) spectrometer, following a similar method as Voliotis et al. (2014).

Modal analysis

While modal analysis has been applied to characterise the size distributions of atmospheric aerosols regarding the physicochemical processes they have been involved in (Hussein et al 2005), this type of analysis is seldom applied to indoor or, more specifically, industrially produced aerosols.

In the present study, NanoScan measurements were expressed as d*N*/dLog*d*p distributions to apply modal analysis, because this method assumes that particle number concentrations are log-normally distributed across their size range. Their distribution can be analysed as three modes: $Mode_{10\text{-}25nm}$, $Mode_{26\text{-}90nm}$, and $Mode_{91\text{-}660nm}$ which includes mainly accumulation mode particles. The algorithm for modal analysis uses a non-linear least square fitting, based on the interior-reflective Newton method (Coleman and Li 1994, 1996). The 3 lognormal fitted curves and their parameters (geometric standard deviation, GSDi; geometric mean diameter, GMDi; and mode number concentration, Ni) were calculated following the same assumptions and conditions as Hussein et al (2005). The modal analysis was performed exclusively on the size-distribution data obtained with NanoScan.

Inhalation model

The inhalation dose of deposited particles in the respiratory system was quantified by multiplying particle size concentrations on the worker area by the ICRP human respiratory tract model deposition probability (Cousins et al 2011). A respiratory volume of 25 L/min was used, which corresponds to male respiration during light exercise (Koivisto et al 2012). The regional dose was calculated for head airways, tracheobronchial and alveolar regions by using simplified deposition fraction equations for the ICRP model as described by Hinds et al.(1999). Particles were assumed to preserve their size during inhalation and the calculation was based on the mobility diameter. Background aerosol particles were assumed to be spherical and to have a density of 1.5 g/cm^3 (Martins et al 2015). The density of particles emitted during thermal spraying was set equal to the density of the feedstock material 4.3 g/cm^3, given that the particles released were found by EDX analysis to have similar composition with the feedstock (see next section). It should be noted that the use of the bulk density of the feedstock material probably overestimates the resulting particle concentrations, because particles may have vaporized and condensed to smaller particles. Results from the NanoScan and MiniWras instruments were combined to obtain a 10 nm-35 μm particle size distribution for the FF (Koivisto et al., 2014). NanoScan size bins between 11.5 - 86.6 nm were used, whereas bins ranging from 139 nm to 35 μm were taken from the MiniWras. Between 86.6 nm and 139 nm a combined channel (108.6 nm) was created.

The particle active surface area was calculated by applying particle size distribution obtained to the equation (1) described by Heitbrink et al. (2009) and Koivisto et al. (2012):

$$s = \frac{3\pi\lambda D_b}{C_c(D_b)\delta} \tag{1}$$

where λ is the mean free path for air, 0.066 μm, and δ is the scattering parameter for air, 0.905. D_b is the mobility diameter and C_c the slip correction factor for the corresponding aerodynamic or

mobility particle size. This calculation refers to particles <700nm according to Heitbrink et al. (2009) and Keller et al. (2001). The particle mass was calculated by using mobility particle diameter and effective density (Koivisto et al 2012):

$$m = \rho_{eff} \frac{\pi}{6} D_b^3 \tag{2}$$

where ρ_{eff} is the effective density (DeCarlo et al 2004). The effective density used was 1.5 g/cm^3 for background particles and 4.3 g/cm^3 for PGNPs.

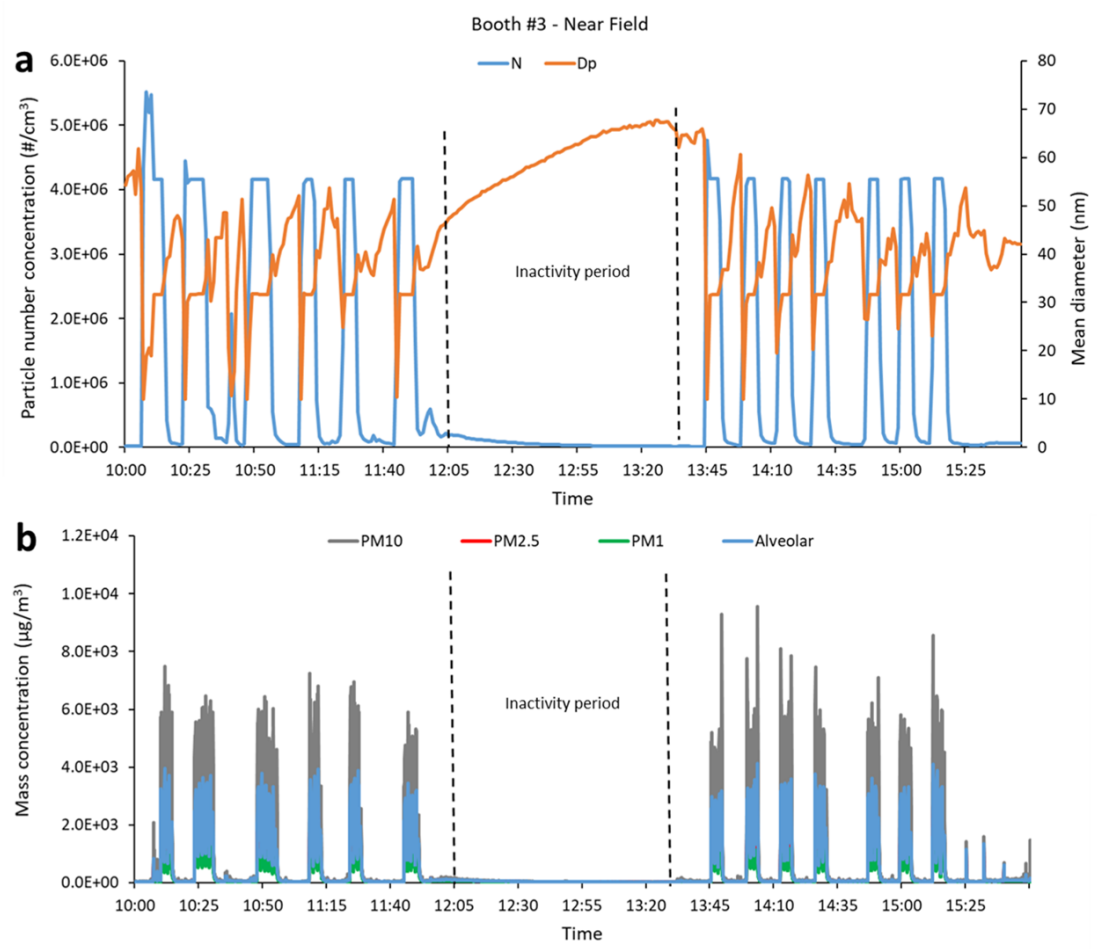

Figure 2. Particle concentrations monitored inside booth #3 (near field) on 26/04/2017 during spraying of feedstock WC/CrC/Ni: (a) particle number concentration and mean diameter; (b) size segregated particle mass concentrations.

Results and Discussion

Particle emissions and impact on exposure

Activities in the thermal spraying facilities were planned by the company for half-day periods. While booth #1 was active during 2 half-days, booths #2 and #3 were operational for 4 half-days each. The data obtained were analysed considering two phases: a pre-process period (background) consisting of the 90-min lunch break when all activity ceased, and the activity periods when particle emissions were simultaneously monitored in the NF and in the FF location. The activity periods were different for each booth (Table 1): while spraying was longer and less repetitive in booth #1 (20-30 min, 3 repetitions/half-day), it had a shorter duration and higher frequency in booth #3 (5-10 min, 7-9 repetitions/half-day). In Booth#2 the spraying activity duration was highly variable (0.5-10 min) and, due to technical problems, there were deviations in the frequency of spraying applications. Hence, the dataset obtained was not representative of regular working days in Booth#2.

In Table 2 average N, D_p, LDSA, and PM_1 values for each of the spraying activities and booths monitored are shown. A representative time series during the process in booth #3 is depicted in Figure 3 (NF) and Figure 4 (FF) during one of the days (26/04/2017), in to order to thoroughly analyse the emission patterns and impacts on exposure of the released NP. The time series for other days and booths are shown in Supplementary Data (Figures S1-S4). In the case of booth #3 each thermal spraying activity lasted for 5-10 minutes (Figure 2); subsequently the worker entered the booth and swapped the metal part which was coated with a new one. The process was repeated to 7-9 times/half-day.

In Figure 2 N, D_p, and size segregated mass concentrations (PM_1, $PM_{2.5}$, PM_{10}, alveolar) values monitored inside booth #3 (NF) are presented. The start of the spraying activity is evident by the rapid increase of N, which exceeded the instrument's (DiSCMini) monitoring range during all

repetitions (maximum N = $4\times10^6/cm^3$). Particle number emissions were directly correlated with decreased D_p, which ranged between 30 and 35 nm during spraying and increased to 45-55 nm between repetitions. The patterns observed for the different spraying activities within each half-day showed good repeatability. N and D_p values during the process (3.8×10^6 /cm^3, 28.6 nm) were markedly different from background aerosols (N< $3.0\times10^4/cm^3$, D_p: 57.5-nm) monitored during the inactivity period on that day (Figure 2, Table 2). The same was true for particle mass concentrations (Figure 2b), which reached up to $4x10^3$ µg/m^3 for the alveolar size fraction (approximately similar to PM_4) while they remained < 30 µg/m^3 during the inactivity period. This result may be attributed to the release of fine and coarse particles (> 1 µm), in addition to NPs, during thermal spraying. The presence of fine and coarse particles was also confirmed by TEM analysis (Figure S5).

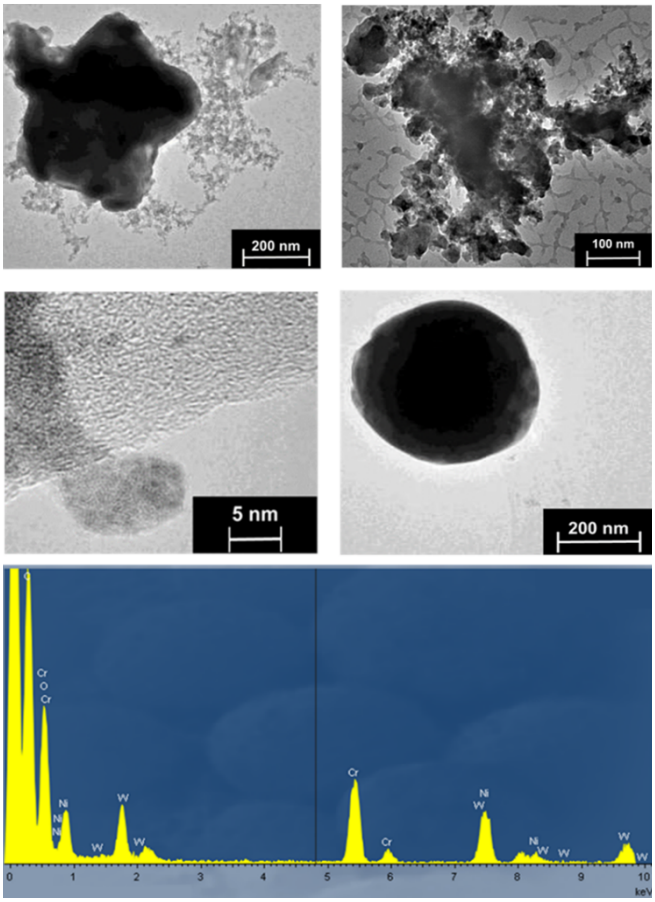

Figure 3. Particles released during spraying of W/CrC/Ni feedstock in booth #3 on 26/04/2017, analysed by TEM and showing similar chemical composition (WC, CrC, Ni) but different morphology and size. EDX spectrum confirming the origin of the particles (WC/CrC/Ni feedstock). The spectrum is representative of particles collected on other TEM grids.

NP emitted during spraying in booth #3 were analysed by TEM (Figure 3), providing evidence that the particles in the collected samples were generated by different mechanisms. Particles collected exhibited a diversity of morphological characteristics, varying both in shape (e.g. spherical, fractal and star-like aggregates) and size (from ca. 5 to 500 nm). Possible emission mechanisms are: mechanical attrition as the feedstock particles crush onto the metal surface with high kinetic energy resulting in irregular-shaped particles, but also melting-evaporation-condensation of the feedstock material which would result in spherical particles (Fonseca et al 2015, Viana et al 2017). EDX analysis of the airborne particles collected on TEM grids confirmed that their chemical composition was similar to that of the feedstock (WC, CrC, Ni), demonstrating that particle release originated from the feedstock and not from other secondary or confounding sources. The thermal spraying processes investigated were not intended to produce nanoparticles. Hence, the NPs emitted from the micro-scaled feedstock (Table S1) were PGNP. In the case of fine and coarse particles, emissions probably resulted when the feedstock particles projected are in the outer plasma stream and do not reach high temperatures, they remain solid and are not deposited effectively on the metal surface.

In the FF location the impact of NP, fine and coarse particle emissions on exposure was assessed in terms of size-resolved N and PM_x (Figure 4). The same repetitive patterns which were monitored inside the spraying booth (Figure 3) were also detected in the worker area, indicating the representativeness of the results as well as clear impacts on exposure. The patterns were different in the morning and afternoon periods because the door of the booth was kept open while spraying during the morning, and closed in the afternoon. *N* values that reached up to $1.7\times10^6/cm^3$ (with the NanoScan instrument), were also outside this instrument's monitoring range and should be considered with high uncertainty. Size-resolved *N* values were highest in the range 20-85 nm (6×10^4 particles/cm^3) during the morning working session, providing evidence that the spraying activities substantially impacted worker exposure. The fact that the personal protective equipment

(FPP3 mask) was frequently removed by the worker as soon as he exited the spraying booth (between repetitions) could further burden the workers' respiratory system. As in the case of the NF, particle concentrations in the FF location were markedly higher during activity than inactivity period. In addition, the effectiveness of keeping the booth door closed as a mitigation strategy was evident: average *N* recorded in the worker area decreased by a factor of 0.31 in the afternoon when the door was closed, and LDSA concentrations were reduced by a factor of 0.38 (Table 2). Hence, the booth´s proper sealing during activity period demonstrated a much larger influence on exposure reduction than the total duration of the activity, or its repetition frequency. Similar findings on the importance of airtight booths had also been reported by Viana et al. (2017) during APS at pilot plant scale.

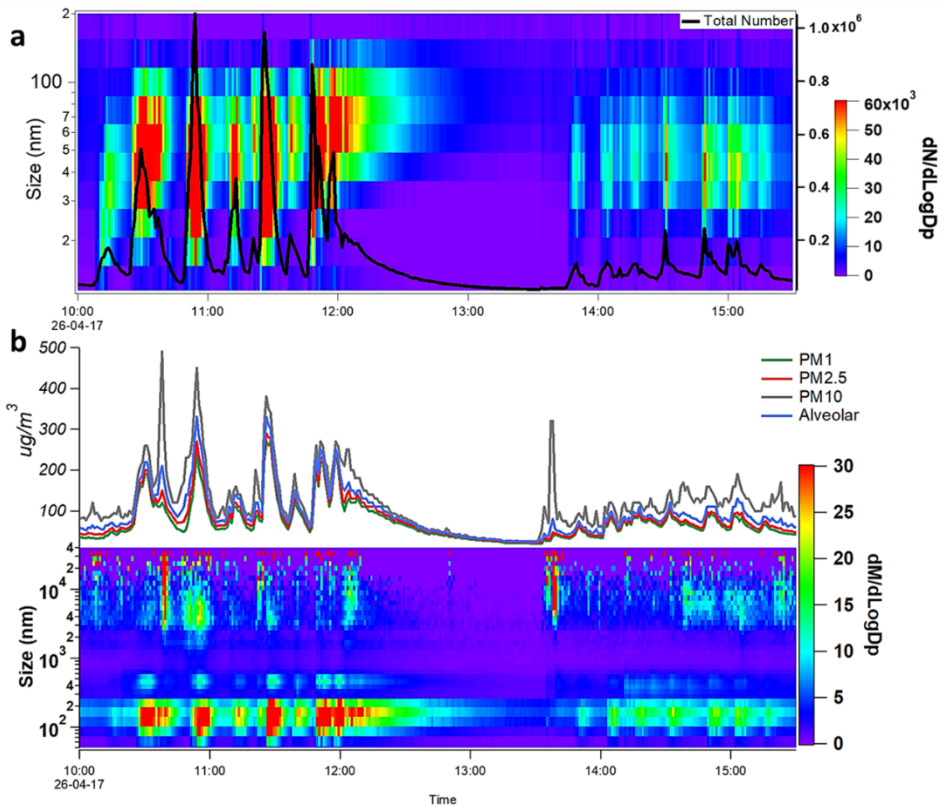

Figure 4. Size-resolved particle concentrations monitored in the worker area (far field) outside booth #3 on 26/04/2017 during spraying of feedstock WC/CrC/Ni: (a) particle number concentrations; (b) particle mass concentrations

In terms of particle mass similar impacts and patterns were observed, although with two particle size modes: 50-500 nm and >3 µm. While the first mode corresponds to PGNP emissions, the second is attributed to direct feedstock release. Alveolar particle mass concentrations reached > 300 µg/m^3 (1-minute means) during the morning activity period, and 150 µg/m^3 in the afternoon.

As shown in Table 2, inside the NF concentrations ranged 1.8-3.4×10^6/cm^3 and had a clear impact on exposure at the FF location, where concentrations in the range of 5.8×10^4-2.0x10^5/cm^3 were monitored, and were significantly higher than the background concentrations (average 3.0×10^4). Concentrations in the FF were above the nano-reference values (NRV, non-regulatory reference values for nanomaterials, based on the precautionary approach) 4×10^4/cm^3 (Van Broekhuizen, et al 2012), and orders of magnitude higher inside the spraying booths (NF). This impact was considered statistically significant following the tiered approach established by Asbach et al. (2012), meaning that exposure concentrations were higher than the background plus 3 times the standard deviation of the background concentrations. The *N*, LDSA and PM values measured were comparable across the different booths, indicating that NP release is activity-dependent and not related to the specific feedstock powders applied. Although different spraying temperatures and velocities were applied in the different booths NP release was evident in all cases. This would indicate that NP emissions are independent of these parameters or that both of the thermal spraying techniques provide the necessary conditions for PGNP emissions.

However, differences in terms of PM_1 ranged from 61 µg/m^3 (booth #1) to 100 µg/m^3 (booth #2) and 640 µg/m^3 (booth #3). These can be attributed to the combination of different process parameters (spraying velocity, speed) of each spraying technique and the different feedstock materials (Cr/Ni and TiO_2/Al_2O_3, Table S1). In the case of booth #1, where two different feedstock powders were applied separately, clear differences were observed in terms of $PM_{2.5}$ (2×10^2 *vs*. 4×10^2 µg/m^3) but not for PM_1 (53 vs. 69 µg/m^3). The feedstock powders applied in booths #2 and #3 were similar (Table S1) resulted in higher PM_1 (100-640 µg/m^3) than in booth #1 (Table 2).

These differences are probably associated with the physical-chemical properties of the feedstock materials rather than to the aggregate size, which as shown in Table S1 is larger for the lowest emitter. As a result, it may be concluded that PM_1emissions were independent of the feedstock and thermal spraying conditions applied, while emissions of coarse particles (>2.5 μm) were influenced by the feedstock. Further research would be necessary to interpret the different behaviour for micron-scaled particle emissions.

With regard to D_p for NP, similarities were detected across booths with particles ranging between 30-40nm in the NF and increasing during transport to 40-64 nm in the FF, where workers were exposed. Workers from other sectors of the facility frequently entered the central area without respiratory protection and were directly exposed to particle concentrations from the spraying booths. As expected, mean diameters during the inactivity period were larger and representative of urban background ultrafine (46-80 nm) aerosols (Reche et al 2015).

Modal distribution and analysis

The modal analysis was applied to the same results dataset as in Figure 4, in FF of booth #3. The time series of the modal particle number concentrations is plotted in Figure 5 for 3 periods: (a) morning activity, (b) midday inactivity period, and (c) afternoon activity. The relative contribution from each mode to total particle number concentrations is also shown for each period.

Modal analysis of particles in the worker area provides information on the size distribution as well as on the potential sources of particles. The $Mode_{26\text{-}90nm}$ was dominant throughout the day in the FF contributing 88-94% of particle number, with the time series of this mode highly resembling the one of total number concentration (Figure 4). New particle formation took place inside the booth (NF, Figure 2), and particles subsequently grew into the larger-sized mode ($Mode_{26\text{-}90nm}$) during their transport from the source towards the worker area (FF, Figure 4a). The relative

contributions from the $Mode_{26\text{-}90nm}$ were similar during the morning (Figure 5a) and afternoon (Figure 5c) spraying activities, despite the differences in total particle number concentrations resulting from the open/closed doors scenarios (Figure 4). $Mode_{10\text{-}25nm}$ were minor contributors with 2-3% during both activity periods, while $Mode_{91\text{-}660nm}$ contributed with 4-9% of relative particle number concentrations.

The lowest contribution of $Mode_{10\text{-}25nm}$ (which includes particles formed by nucleation) in terms of particle number release was recorded during the inactivity period (Figure 5b) as expected due to the absence of activities in the facility. $Mode_{91\text{-}660nm}$ showed the highest contribution during the morning activity (Figure 5a) due to the influence of the open door.

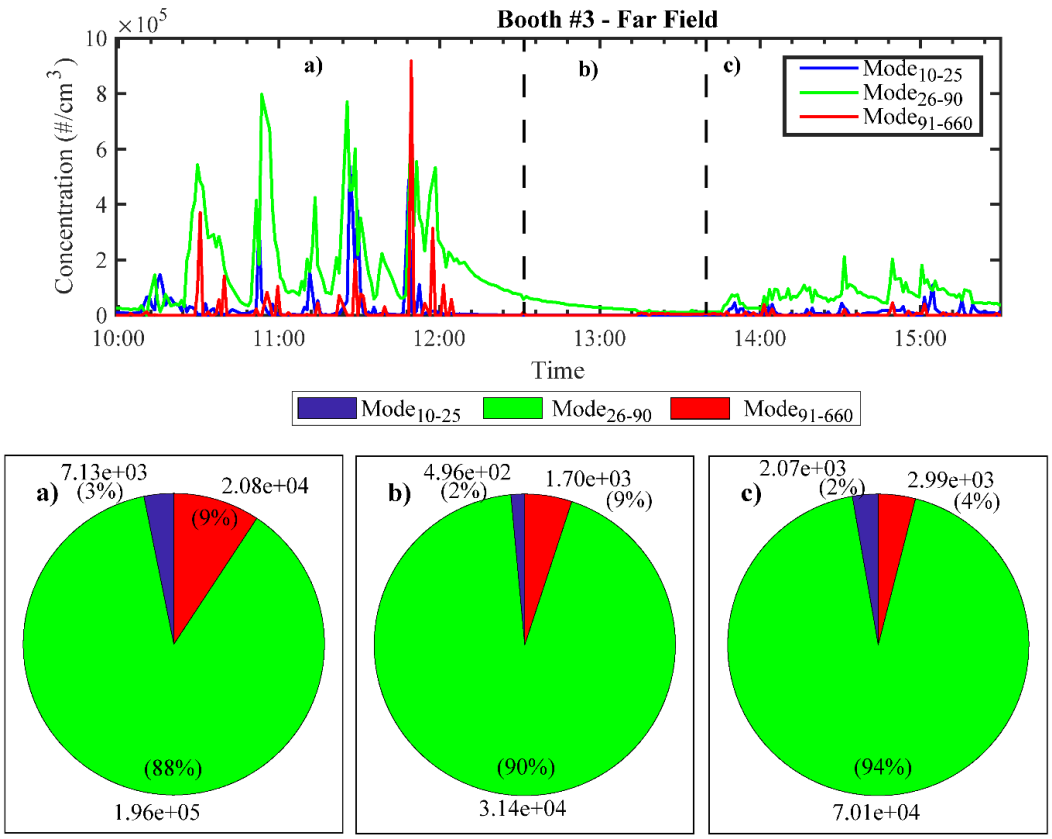

Figure 5. Particle number concentrations for particles in each of the modes identified by modal analysis (top) for booth #3 data for 26/04/2017. Absolute average number concentration and relative contribution (%) of each mode (bottom) for time intervals (a) morning, (b) inactivity period, and (c) afternoon.

Certain considerations should be taken into account in the application of modal analysis to the occupational dataset presented in this work Particles deriving from nucleation can have sizes from 1 nm, while very few instruments are able to measure particles in this size range. The instrumentation used in this work had a lower cutoff at 10 nm (NanoScan) which results in an underestimation of the $Mode_{10\text{-}25}$ contributions. The same is probably true for the $Mode_{91\text{-}660nm}$, given that the instruments had an upper cutoff size at 420 nm. The underestimation of the $Mode_{91\text{-}660nm}$ mode was probably lower since the number of particles in the range 420-660 nm emitted during thermal spraying is low.

Calculated deposited dose during inhalation

Inhalation dose rates for particle number, surface area and mass were estimated for booth #3 (26/04/2017 and 28/04/2017), for each half-day (morning and afternoon) and midday inactivity period for the FF location (Table 3), where workers carried out different tasks and the use of personal protection equipment was limited. Particle number dose rates ($\dot{n}$) were higher during activity (353×10^6 to 1024×10^6/min) than during inactivity periods (138×10^6 to 374×10^6/min). During the spraying activity, approximately 70% of the total inhaled particle number concentrations was deposited in the alveolar region, 12% in the trachea bronchi and 18% in the head airways. Hence, for workers in the FF location 82% of the total inhaled particles sourcing from thermal spraying were deposited in the deepest regions of the respiratory tract.

The same analysis was applied to the calculated active surface area concentrations of the particles deposited in the airways ($\dot{s}$) during activity periods (3.0 – 6.3×10^6 $\mu m^2/min^1$, Table 3): 60% was estimated to be deposited in the alveolar region, 9% in the trachea bronchi, and 31% in the head airways. Total surface area of the deposited particles during activity was higher than during inactivity (1.8×10^6 μm^2/min). The LDSA concentrations in this study (1.2-5.6 $\times10^3$ $\mu m^2/cm^3$,

FF, Table 2) were mostly higher than others found in the literature, where LDSA concentrations were on average 21.6 $\mu m^2/cm^3$ during handling and loading of halloysite nanotubes (Koivisto et al., 2018), and <19 $\mu m^2/cm^3$during WC-Co fine powder production (Koivisto et al., 2016). Regarding the total deposited mass ($\dot{m}$), increases of 1-9.5 ng/min were calculated from inactivity to activity periods. These dose rates in terms of mass were higher than those reported by Koivisto et al. (2014) (0.03-0.53 ng/min) during a lab-scale exposure assessment to nanodiamonds.

Koivisto et al (2012), who found comparable results to those in the current work during a high energy process (Liquid Flame Spray), concluded that N was the most relevant metric for exposure assessment. However, biologically, the most relevant metric considering pulmonary inflammation is likely surface area (Schmid and Stoeger 2017).

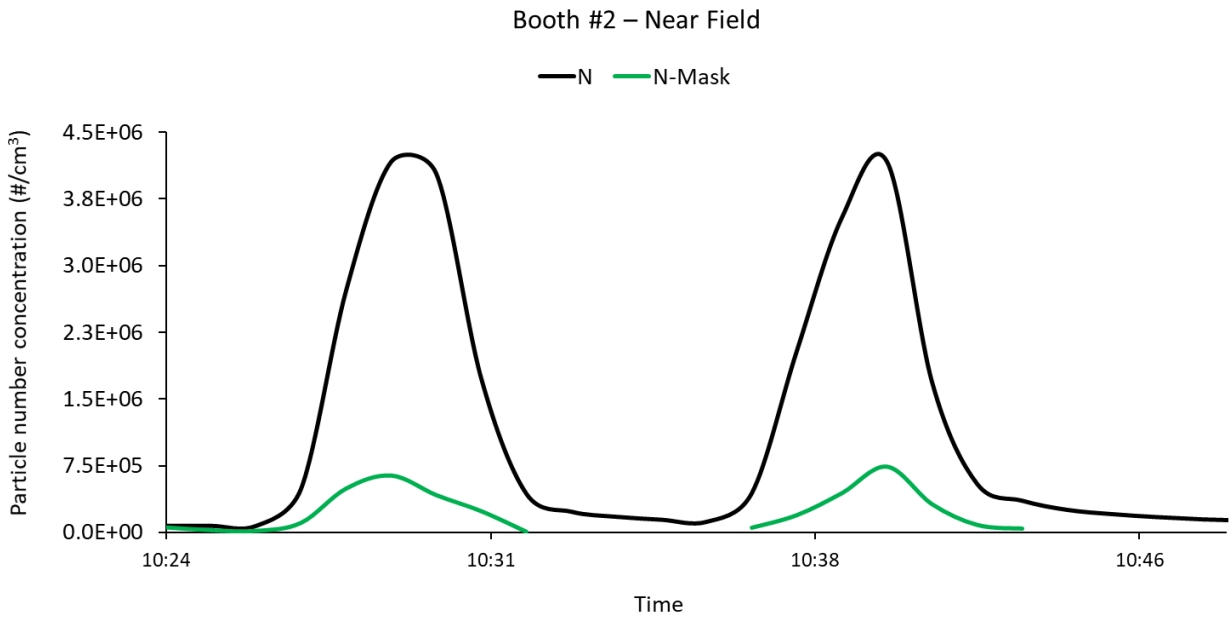

Figure 6. Particle number concentration and mean diameters measured with DiSCMini inside and outside an FPP3 personal mask worn by a volunteer-member of the research team. Measurements took place in the near field during two activity periods in booth #2 (27-04-2017).

Effectiveness of protective personal equipment

The effectiveness of a personal FPP3 respirator (Moldex Air Plus 3405, half-piece mask) was assessed on a case study basis by comparing measurements obtained simultaneously inside and outside the respirator, with two DiSCMini units, while the mask was worn by one volunteer-member of the research team. The respirator assigned protection factor (APF) was 10 as specified by the 29 CFR 1910.134 (Occupational Safety and Health Admin. 2006). Programme protection factors (PPFs) were studied by Koivisto et al (2015) for loose-fitting respirators. The measurements were carried out inside booth #2 (NF) and during two representative activity periods. The inlet of one of the instruments was held in the breathing zone (outside the mask), and the second was connected to the interior of the mask with Tygon conductive tubing (Asbach et al 2016).

The particle concentrations monitored (Figure 6) show that the mask achieved a reduction of worker exposure in terms of number concentration by 87% (from 3×10^6 to $4\times10^5/cm^3$) on average for both activity periods. This is likely a conservative estimate since the inlet of the instrument prevented from achieving a proper fit of the mask and it is highly probable that unfiltered air entered in the mask and interfered with the measurements.

Conclusions

Particle emissions and impacts on exposure were monitored for NPs and micron-scaled particles (fine and coarse) in terms of particle number and mass concentrations, LDSA, mean diameter and size distributions, during the application of ceramic coatings on metal surfaces by means of thermal spraying, at industrial scale. The results obtained are representative of the industrial facility under study, which has unique characteristics as most industrial facilities do, which highlights the need for additional studies with this kind of focus in the literature. Results may only

be generalized once the body of literature regarding industrial thermal spraying emissions and the influence of different feedstock materials become available.

High particle number (>10^6/cm^3) and mass (60-600 µgPM_1/m^3) concentrations were recorded inside the thermal spraying booths (NF), which were transported towards the worker area (FF) increasing the FF concentrations by one order of magnitude in terms of N (10^4-10^5/cm^3) and up to a factor of 4 in PM1 (44-100 µg/m^3). NPs were generated through different mechanisms (mechanical, melting-condensation), resulting in diverse morphologies (irregular, spherical). NPs with small diameters were detected inside (31-41 nm) and outside (40-64 nm) the spraying booths. Worker exposure occurred both in the NF and FF locations, given that the workers operated equally inside and outside the spraying booths. The inhalation model applied showed that particles emitted during thermal spraying were mainly deposited in the alveolar region (70%).

The high correlation between particle concentrations in the NF and FF suggest that worker exposure was strongly impacted by NPs, fine and coarse particles emitted during thermal spraying. Whereas similar NP number concentrations were monitored irrespective of the spraying technique and feedstock material applied, coarser particle (>2.5 µm) mass concentrations showed differences as a function of the feedstock material. Additional research is necessary to understand the relationship between coarse particle emissions and feedstock physical-chemical properties.

The advantages and limitations of applying modal analysis to an occupational dataset were assessed. This analysis allowed for the identification of a dominant mode ($Mode_{26\text{-}90}$ particles, 89%), the increased contribution from $Mode_{10\text{-}25nm}$ (nucleation) particles during thermal spraying periods, and the influence of outdoor urban background aerosols during the inactivity period. In spite of the continuously working local extraction systems, the proper sealing of the spraying booths was identified as a key element for exposure reduction. Differences in exposure concentrations of one order of magnitude (from 10^5/cm^3 to 10^4/cm^3) were recorded when doors

were open/closed. Optimising the production routine to prevent the opening of doors during the spraying activity as well as a delayed door-opening protocol could reduce NP transport from inside the booths and consequently minimise impacts on exposure in the adjacent worker areas. Furthermore, worker access in the central area should be restricted during spraying operation, or carried out with adequate personal protective equipment (PPE). Finally, the use of FPP3 masks (with APF 10) was also advised, given their high potential for reduction of particle number concentrations.

Acknowledgements

The current work was carried out in the framework of the CERASAFE project (www.cerasafe.eu), with the support of SIINN ERA-NET (project id: 16), and was funded by the Spanish MINECO (PCIN-2015-173-C02-01) and the Romanian UEFISCDI (PN-III-P4-ID-PCE-2016-0835). Partial funding from the “Generalitat de Catalunya” (project number: AGAUR 2017 SGR41) is also acknowledged. The authors kindly acknowledge TM COMAS (http://www.tmcomas.com) for their committed cooperation.

REFERENCES

Araujo JA, Barajas B, Kleinman M, Wang X, Bennett BJ, Gong KW, Navab M, Harkema J, Sioutas C, Lusis AJ and Nel AE (2008) Ambient particulate pollutants in the ultrafine range promote early atherosclerosis and systemic oxidative stress. *Circulation Research* 102(5): 589–596.

Asbach C, Kaminski H, Lamboy Y, Schneiderwind U, Fierz M and Todea AM (2016) Silicone sampling tubes can cause drastic artifacts in measurements with aerosol instrumentation based on unipolar diffusion charging. *Aerosol Science and Technology* 50(12): 1375–1384.

Asbach C, Kuhlbusch T a J, Kaminski H, Plitzko S, Götz U, Voetz M and Dahmann D (2012) *Authors : SOP-Tiered Approach Tiered Approach for the assessment of exposure to airborne nanoobjects in work- places*. .

Baiamonte L, Marra F, Gazzola S, Giovanetto P, Bartuli C, Valente T and Pulci G (2015) Thermal sprayed coatings for hot corrosion protection of exhaust valves in naval diesel engines. *Surface and Coatings Technology*. Elsevier B.V. 295: 78–87. Available at: http://dx.doi.org/10.1016/j.surfcoat.2015.10.072.

Bémer D, Régnier R, Subra I, Sutter B, Lecler MT and Morele Y (2010) Ultrafine Particles Emitted by Flame and Electric Arc Guns for Thermal Spraying of Metals. *The Annals of Occupational Hygiene* 54(6): 607–614.

Van Broekhuizen P, Van Veelen W, Streekstra WH, Schulte P and Reijnders L (2012) Exposure limits for nanoparticles: Report of an international workshop on nano reference values. *Annals of Occupational Hygiene* 56(5): 515–524.

Coleman TF and Li Y (1994) On the convergence of interior-reflective Newton methods for nonlinear minimization subject to bounds. *Mathematical Programming* 67(1–3): 189–224.

Coleman TF and Li Y (1996) An Interior Trust Region Approach for Nonlinear Minimization Subject to Bounds. *SIAM Journal on Optimization* 6(2): 418–445. Available at: https://doi.org/10.1137/0806023.

Cousins C, Boice Jr JD, Cooper UJR, Lee UJ and Lochard KJ (2011) Annals of the ICRP Published on behalf of the International Commission on Radiological Protection International Commission on Radiological Protection Members of the 2010–2013 Main Commission of ICRP. . Available at: http://www.icrp.org/docs/P.

DeCarlo PF, Slowik JG, Stainken K, Davidovits P, Williams LR, Jayne JT, Kolb CE, Worsnop DR, Rudich Y and Jimenez JL (2004) Particle morphology and density characterization by combined mobility and aerodynamic diameter measurements. Part 2: Application to combustion-generated soot aerosols as a function of fuel equivalence ratio. *Aerosol Science and Technology* 38(12): 1206–1222.

Ding Y, Kuhlbusch TAJ, Van Tongeren M, Jiménez AS, Tuinman I, Chen R, Alvarez IL, Mikolajczyk U, Nickel C, Meyer J, Kaminski H, Wohlleben W, Stahlmecke B, Clavaguera S and Riediker M (2017) Airborne engineered nanomaterials in the workplace—a review of release and worker exposure during nanomaterial production and handling processes. *Journal of Hazardous Materials* 322: 17–28.

Fonseca AS, Kuijpers E, Kling KI, Levin M, Koivisto AJ, Nielsen SH, Fransman W, Fedutik Y, Jensen KA and Koponen IK (2018) Particle release and control of worker exposure during laboratory-scale synthesis, handling and simulated spills of manufactured nanomaterials in fume hoods. *Journal of Nanoparticle Research*. Journal of Nanoparticle Research 20(2).

Fonseca AS, Maragkidou A, Viana M, Querol X, Hämeri K, de Francisco I, Estepa C, Borrell C, Lennikov V and de la Fuente GF (2016) Process-generated nanoparticles from ceramic tile sintering: Emissions, exposure and environmental release. *Science of the Total Environment*

565: 922–932.

Fonseca AS, Viana M, Querol X, Moreno N, de Francisco I, Estepa C and de la Fuente GF (2015) Ultrafine and nanoparticle formation and emission mechanisms during laser processing of ceramic materials. *Journal of Aerosol Science* 88: 48–57.

Fujitani Y, Kobayashi T, Arashidani K, Kunugita N and Suemura K (2008) Measurement of the physical properties of aerosols in a fullerene factory for inhalation exposure assessment. *Journal of Occupational and Environmental Hygiene* 5(6): 380–389.

Gakidou E, Afshin A, Abajobir AA, Abate KH, Abbafati C, Abbas KM, Abd-Allah F, Abdulle AM, Abera SF, Aboyans V, Abu-Raddad LJ, Abu-Rmeileh NME, Abyu GY, Adedeji IA, Adetokunboh O, Afarideh M, Agrawal A, Agrawal S, Ahmad Kiadaliri A, Ahmadieh H, Ahmed MB, Aichour AN, Aichour I, Aichour MTE, Akinyemi RO, Akseer N, Alahdab F, Al-Aly Z, Alam K, Alam N, Alam T, Alasfoor D, Alene KA, Ali K, Alizadeh-Navaei R, Alkerwi A, Alla F, Allebeck P, Al-Raddadi R, Alsharif U, Altirkawi KA, Alvis-Guzman N, Amare AT, Amini E, Ammar W, Amoako YA, Ansari H, Antó JM, Antonio CAT, Anwari P, Arian N, Ärnlöv J, Artaman A, Aryal KK, Asayesh H, Asgedom SW, Atey TM, Avila-Burgos L, Avokpaho EFGA, Awasthi A, Azzopardi P, Bacha U, Badawi A, Balakrishnan K, Ballew SH, Barac A, Barber RM, Barker-Collo SL, Bärnighausen T, Barquera S, Barregard L, Barrero LH, Batis C, Battle KE, Baune BT, Beardsley J, Bedi N, Beghi E, Bell ML, Bennett DA, Bennett JR, Bensenor IM, Berhane A, Berhe DF, Bernabé E, Betsu BD, Beuran M, Beyene AS, Bhansali A, Bhutta ZA, Bikbov B, Birungi C, Biryukov S, Blosser CD, Boneya DJ, Bou-Orm IR, Brauer M, Breitborde NJK, Brenner H, Brugha TS, Bulto LNB, Baumgarner BR, Butt ZA, Cahuana-Hurtado L, Cárdenas R, Carrero JJ, Castañeda-Orjuela CA, Catalá-López F, Cercy K, Chang HY, Charlson FJ, Chimed-Ochir O, Chisumpa VH, Chitheer AA, Christensen H, Christopher DJ, Cirillo M, Cohen AJ, Comfort H, Cooper C, Coresh J, Cornaby L, Cortesi PA, Criqui MH, Crump JA, Dandona L, Dandona R, Das Neves J, Davey G, Davitoiu D V., Davletov K, De Courten B, Degenhardt L, Deiparine S, Dellavalle RP, Deribe K,

Deshpande A, Dharmaratne SD, Ding EL, Djalalinia S, Do HP, Dokova K, Doku DT, Dorsey ER, Driscoll TR, Dubey M, Duncan BB, Duncan S, Ebert N, Ebrahimi H, El-Khatib ZZ, Enayati A, Endries AY, Ermakov SP, Erskine HE, Eshrati B, Eskandarieh S, Esteghamati A, Estep K, Faraon EJA, Farinha CSES, Faro A, Farzadfar F, Fay K, Feigin VL, Fereshtehnejad SM, Fernandes JC, Ferrari AJ, Feyissa TR, Filip I, Fischer F, Fitzmaurice C, Flaxman AD, Foigt N, Foreman KJ, Frostad JJ, Fullman N, Fürst T, Furtado JM, Ganji M, Garcia-Basteiro AL, Gebrehiwot TT, Geleijnse JM, Geleto A, Gemechu BL, Gesesew HA, Gething PW, Ghajar A, Gibney KB, Gill PS, Gillum RF, Giref AZ, Gishu MD, Giussani G, Godwin WW, Gona PN, Goodridge A, Gopalani SV, Goryakin Y, Goulart AC, Graetz N, Gugnani HC, Guo J, Gupta R, Gupta T, Gupta V, Gutiérrez RA, Hachinski V, Hafezi-Nejad N, Hailu GB, Hamadeh RR, Hamidi S, Hammami M, Handal AJ, Hankey GJ, Harb HL, Hareri HA, Hassanvand MS, Havmoeller R, Hawley C, Hay SI, Hedayati MT, Hendrie D, Heredia-Pi IB, Hoek HW, Horita N, Hosgood HD, Hostiuc S, Hoy DG, Hsairi M, Hu G, Huang H, Huang JJ, Iburg KM, Ikeda C, Inoue M, Irvine CMS, Jackson MD, Jacobsen KH, Jahanmehr N, Jakovljevic MB, Jauregui A, Javanbakht M, Jeemon P, Johansson LRK, Johnson CO, Jonas JB, Jürisson M, Kabir Z, Kadel R, Kahsay A, Kamal R, Karch A, Karema CK, Kasaeian A, Kassebaum NJ, Kastor A, Katikireddi SV, Kawakami N, Keiyoro PN, Kelbore SG, Kemmer L, Kengne AP, Kesavachandran CN, Khader YS, Khalil IA, Khan EA, Khang YH, Khosravi A, Khubchandani J, Kieling C, Kim D, Kim JY, Kim YJ, Kimokoti RW, Kinfu Y, Kisa A, Kissimova-Skarbek KA, Kivimaki M, Knibbs LD, Knudsen AK, Kopec JA, Kosen S, Koul PA, Koyanagi A, Kravchenko M, Krohn KJ, Kromhout H, Kuate Defo B, Kucuk Bicer B, Kumar GA, Kutz M, Kyu HH, Lal DK, Lalloo R, Lallukka T, Lan Q, Lansingh VC, Larsson A, Lee A, Lee PH, Leigh J, Leung J, Levi M, Li Y, Li Y, Liang X, Liben ML, Linn S, Liu P, Lodha R, Logroscino G, Looker KJ, Lopez AD, Lorkowski S, Lotufo PA, Lozano R, Lunevicius R, Macarayan ERK, Magdy Abd El Razek H, Magdy Abd El Razek M, Majdan M, Majdzadeh R, Majeed A, Malekzadeh R, Malhotra R, Malta DC, Mamun AA, Manguerra H, Mantovani LG, Mapoma CC, Martin R V., Martinez-Raga J, Martins-Melo FR, Mathur MR,

Matsushita K, Matzopoulos R, Mazidi M, McAlinden C, McGrath JJ, Mehata S, Mehndiratta MM, Meier T, Melaku YA, Memiah P, Memish ZA, Mendoza W, Mengesha MM, Mensah GA, Mensink GBM, Mereta ST, Meretoja A, Meretoja TJ, Mezgebe HB, Micha R, Millear A, Miller TR, Minnig S, Mirarefin M, Mirrakhimov EM, Misganaw A, Mishra SR, Mohammad KA, Mohammed KE, Mohammed S, Mohamed Ibrahim N, Mohan MBV, Mokdad AH, Monasta L, Montañez Hernandez JC, Montico M, Moradi-Lakeh M, Moraga P, Morawska L, Morrison SD, Mountjoy-Venning C, Mueller UO, Mullany EC, Muller K, Murthy GVS, Musa KI, Naghavi M, Naheed A, Nangia V, Natarajan G, Negoi I, Negoi RI, Nguyen CT, Nguyen G, Nguyen M, Nguyen Q Le, Nguyen TH, Nichols E, Ningrum DNA, Nomura M, Nong VM, Norheim OF, Norrving B, Noubiap JJN, Obermeyer CM, Ogbo FA, Oh IH, Oladimeji O, Olagunju AT, Olagunju TO, Olivares PR, Olsen HE, Olusanya BO, Olusanya JO, Opio JN, Oren E, Ortiz A, Ota E, Owolabi MO, Pa M, Pacella RE, Pana A, Panda BK, Panda-Jonas S, Pandian JD, Papachristou C, Park EK, Parry CD, Patten SB, Patton GC, Pereira DM, Perico N, Pesudovs K, Petzold M, Phillips MR, Pillay JD, Piradov MA, Pishgar F, Plass D, Pletcher MA, Polinder S, Popova S, Poulton RG, Pourmalek F, Prasad N, Purcell C, Qorbani M, Radfar A, Rafay A, Rahimi-Movaghar A, Rahimi-Movaghar V, Rahman M, Rahman MHU, Rahman MA, Rai RK, Rajsic S, Ram U, Rawaf S, Rehm CD, Rehm J, Reiner RC, Reitsma MB, Reynales-Shigematsu LM, Remuzzi G, Renzaho AMN, Resnikoff S, Rezaei S, Ribeiro AL, Rivera JA, Roba KT, Rojas-Rueda D, Roman Y, Room R, Roshandel G, Roth GA, Rothenbacher D, Rubagotti E, Rushton L, Sadat N, Safdarian M, Safi S, Safiri S, Sahathevan R, Salama J, Salomon JA, Samy AM, Sanabria JR, Sanchez-Niño MD, Sánchez-Pimienta TG, Santomauro D, Santos IS, Santric Milicevic MM, Sartorius B, Satpathy M, Sawhney M, Saxena S, Schaeffner E, Schmidt MI, Schneider IJC, Schutte AE, Schwebel DC, Schwendicke F, Seedat S, Sepanlou SG, Serdar B, Servan-Mori EE, Shaddick G, Shaheen A, Shahraz S, Shaikh MA, Shamah Levy T, Shamsipour M, Shamsizadeh M, Shariful Islam SM, Sharma J, Sharma R, She J, Shen J, Shi P, Shibuya K, Shields C, Shiferaw MS, Shigematsu M, Shin MJ, Shiri R, Shirkoohi R, Shishani K, Shoman H,

Shrime MG, Sigfusdottir ID, Silva DAS, Silva JP, Silveira DGA, Singh JA, Singh V, Sinha DN, Skiadaresi E, Slepak EL, Smith DL, Smith M, Sobaih BHA, Sobngwi E, Soneji S, Sorensen RJD, Sposato LA, Sreeramareddy CT, Srinivasan V, Steel N, Stein DJ, Steiner C, Steinke S, Stokes MA, Strub B, Subart M, Sufiyan MB, Suliankatchi RA, Sur PJ, Swaminathan S, Sykes BL, Szoeke CEI, Tabarés-Seisdedos R, Tadakamadla SK, Takahashi K, Takala JS, Tandon N, Tanner M, Tarekegn YL, Tavakkoli M, Tegegne TK, Tehrani-Banihashemi A, Terkawi AS, Tesssema B, Thakur JS, Thamsuwan O, Thankappan KR, Theis AM, Thomas ML, Thomson AJ, Thrift AG, Tillmann T, Tobe-Gai R, Tobollik M, Tollanes MC, Tonelli M, Topor-Madry R, Torre A, Tortajada M, Touvier M, Tran BX, Truelsen T, Tuem KB, Tuzcu EM, Tyrovolas S, Ukwaja KN, Uneke CJ, Updike R, Uthman OA, Van Boven JFM, Van Donkelaar A, Varughese S, Vasankari T, Veerman LJ, Venkateswaran V, Venketasubramanian N, Violante FS, Vladimirov SK, Vlassov VV, Vollset SE, Vos T, Wadilo F, Wakayo T, Wallin MT, Wang YP, Weichenthal S, Weiderpass E, Weintraub RG, Weiss DJ, Werdecker A, Westerman R, Whiteford HA, Wiysonge CS, Woldeyes BG, Wolfe CDA, Woodbrook R, Workicho A, Wulf Hanson S, Xavier D, Xu G, Yadgir S, Yakob B, Yan LL, Yaseri M, Yimam HH, Yip P, Yonemoto N, Yoon SJ, Yotebieng M, Younis MZ, Zaidi Z, El Sayed Zaki M, Zavala-Arciniega L, Zhang X, Zimsen SRM, Zipkin B, Zodpey S, Lim SS and Murray CJL (2017) Global, regional, and national comparative risk assessment of 84 behavioural, environmental and occupational, and metabolic risks or clusters of risks, 1990-2016: A systematic analysis for the Global Burden of Disease Study 2016. *The Lancet* 390(10100): 1345–1422.

Ganser GH and Hewett P (2017) Models for nearly every occasion: Part II - Two box models. *Journal of Occupational and Environmental Hygiene* 14: 58–71.

Gérard B (2006) Application of thermal spraying in the automobile industry. *Surface and Coatings Technology* 201(5): 2028–2031.

Hallé S, Nadeau S and Fatisson J (2015) Engineered containment and control of airborne

nanoparticles: Current status. *International Journal of Safety and Security Engineering* 5(4): 336–351.

Heitbrink WA, Evans DE, Ku BK, Maynard AD, Slavin TJ and Peters TM (2009) Relationships among particle number, surface area, and respirable mass concentrations in automotive engine manufacturing. *Journal of Occupational and Environmental Hygiene* 6(1): 19–31. Available at: http://www.tandfonline.com/doi/abs/10.1080/15459620802530096.

Hériaud-Kraemer H, Montavon G, Coddet C, Hertert S and Robin H (2003) Harmful risks for workers in thermal spraying: A review completed by a survey in a French company. *Journal of Thermal Spray Technology* 12(4): 542–554.

Hewett P and Ganser GH (2017) Models for nearly every occasion: Part I - One box models. *Journal of Occupational and Environmental Hygiene*. Taylor & Francis 14(1): 49–57.

Hinds WC (1999) *Aerosol technology: Properties, Behavior, and Measurement of Airborne Particles. Wiley-Interscience Publication*. Wiley. Available at: https://books.google.es/books/about/Aerosol_technology.html?id=ORxSAAAAMAAJ&redir_esc=y.

Hoek G, Boogaard H, Knol A, De Hartog J, Slottje P, Ayres JG, Borm P, Brunekreef B, Donaldson K, Forastiere F, Holgate S, Kreyling WG, Nemery B, Pekkanen J, Stone V, Wichmann HE and Van Der Sluijs J (2010) Concentration response functions for ultrafine particles and all-cause mortality and hospital admissions: Results of a European expert panel elicitation. *Environmental Science and Technology* 44(1): 476–482.

Huang H, Li H and Li X (2016) Physicochemical Characteristics of Dust Particles in HVOF Spraying and Occupational Hazards: Case Study in a Chinese Company. *Journal of Thermal Spray Technology*. Springer US 25(5): 971–981.

Hussein T, Hämeri K, Aalto PP, Paatero P and Kulmala M (2005) Modal structure and spatial-temporal variations of urban and suburban aerosols in Helsinki - Finland. *Atmospheric Environment* 39(9): 1655–1668.

Hussein T, Maso MD, Petäjä T, Koponen IK, Paatero P, Aalto PP, Hämeri K and Kulmala M (2005) Evaluation of an automatic algorithm for fitting the particle number size distributions. *Boreal Environment Research.* 10(October): 337–355.

Ibald-Mulli A, Wichmann H-E, Kreyling W and Peters A (2002) Epidemiological Evidence on Health Effects of Ultrafine Particles. *Journal of Aerosol Medicine* 15(2): 189–201. Available at: http://www.liebertonline.com/doi/abs/10.1089/089426802320282310.

Keller A, Fierz M, Siegmann K, Siegmann HC and Filippov A (2001) Surface science with nanosized particles in a carrier gas. *Journal of Vacuum Science & Technology A* 19(1): 1–8. Available at: https://doi.org/10.1116/1.1339832.

Knibbs LD, Cole-Hunter T and Morawska L (2011) A review of commuter exposure to ultrafine particles and its health effects. *Atmospheric Environment*. Elsevier Ltd 45(16): 2611–2622. Available at: http://dx.doi.org/10.1016/j.atmosenv.2011.02.065.

Koivisto AJ, Aromaa M, Koponen IK, Fransman W, Jensen KA, Mäkelä JM and Hämeri KJ (2015) Workplace performance of a loose-fitting powered air purifying respirator during nanoparticle synthesis. *Journal of Nanoparticle Research* 17(4).

Koivisto AJ, Aromaa M, Mäkelä JM, Pasanen P, Hussein T and Hämeri K (2012) Concept To Estimate Regional Inhalation Dose of Industrially Synthesized Nanoparticles. *ACSNano* 6: 1195–1203.

Koivisto AJ, Bluhme AB, Kling KI, Fonseca AS, Redant E, Andrade F, Hougaard KS, Krepker M, Prinz OS, Segal E, Holländer A, Jensen KA, Vogel U and Koponen IK (2018) Occupational

exposure during handling and loading of halloysite nanotubes – A case study of counting nanofibers. *NanoImpact* 10(April): 153–160.

Koivisto AJ, Jensen ACØ, Levin M, Kling KI, Maso MD, Nielsen SH, Jensen KA and Koponen IK (2015) Testing the near field/far field model performance for prediction of particulate matter emissions in a paint factory. *Environmental Science: Processes & Impacts*. Royal Society of Chemistry 17(1): 62–73. Available at: http://xlink.rsc.org/?DOI=C4EM00532E.

Koivisto AJ, Kling KI, Levin M, Fransman W, Gosens I, Cassee FR and Jensen KA (2016) First order risk assessment for nanoparticle inhalation exposure during injection molding of polypropylene composites and production of tungsten-carbide-cobalt fine powder based upon pulmonary inflammation and surface area dose. *NanoImpact*. The Authors 6: 30–38. Available at: http://dx.doi.org/10.1016/j.impact.2016.11.002.

Koivisto AJ, Palomäki JE, Viitanen AK, Siivola KM, Koponen IK, Yu M, Kanerva TS, Norppa H, Alenius HT, Hussein T, Savolainen KM and Hämeri KJ (2014) Range-finding risk assessment of inhalation exposure to nanodiamonds in a laboratory environment. *International Journal of Environmental Research and Public Health* 11(5): 5382–5402.

Koponen IK, Koivisto AJ and Jensen KA (2015) Worker exposure and high time-resolution analyses of process-related submicrometre particle concentrations at mixing stations in two paint factories. *Annals of Occupational Hygiene* 59(6): 749–763.

Kuhlbusch TAJ, Neumann S and Fissan H (2004) Number Size Distribution, Mass Concentration, and Particle Composition of PM_1, $PM_{2.5}$, and PM_{10} in Bag Filling Areas of Carbon Black Production. *Journal of Occupational and Environmental Hygiene* 1(10): 660–671. Available at: http://www.tandfonline.com/doi/abs/10.1080/15459620490502242.

Landrigan PJ, Fuller R, Acosta NJR, Adeyi O, Arnold R, Basu N, Baldé AB, Bertollini R, Bose-O'Reilly S, Boufford JI, Breysse PN, Chiles T, Mahidol C, Coll-Seck AM, Cropper ML, Fobil J,

Fuster V, Greenstone M, Haines A, Hanrahan D, Hunter D, Khare M, Krupnick A, Lanphear B, Lohani B, Martin K, Mathiasen K V., McTeer MA, Murray CJL, Ndahimananjara JD, Perera F, Potočnik J, Preker AS, Ramesh J, Rockström J, Salinas C, Samson LD, Sandilya K, Sly PD, Smith KR, Steiner A, Stewart RB, Suk WA, van Schayck OCP, Yadama GN, Yumkella K and Zhong M (2017) The Lancet Commission on pollution and health. *The Lancet* 391.

Lima RS and Marple BR (2006) From APS to HVOF spraying of conventional and nanostructured titania feedstock powders: A study on the enhancement of the mechanical properties. *Surface and Coatings Technology* 200(11): 3428–3437.

Losert S, von Goetz N, Bekker C, Fransman W, Wijnhoven SWP, Delmaar C, Hungerbuhler K and Ulrich A (2014) Human Exposure to Conventional and Nanoparticle-Containing Sprays—A Critical Review. *Environmental Science & Technology*. American Chemical Society 48(10): 5366–5378.

Martins V, Cruz Minguillón M, Moreno T, Querol X, de Miguel E, Capdevila M, Centelles S and Lazaridis M (2015) Deposition of aerosol particles from a subway microenvironment in the human respiratory tract. *Journal of Aerosol Science*. Elsevier 90: 103–113. Available at: http://dx.doi.org/10.1016/j.jaerosci.2015.08.008.

Maynard AD, Aitken RJ, Butz T, Colvin V, Donaldson K, Oberdörster G, Philbert MA, Ryan J, Seaton A, Stone V, Tinkle SS, Tran L, Walker NJ and Warheit DB (2006) Safe handling of nanotechnology. *Nature*. Nature Publishing Group 444: 267. Available at: http://dx.doi.org/10.1038/444267a.

Moskowitz LN (1993) Application of HVOF thermal spraying to solve corrosion problems in the petroleum industry-an industrial note. *Journal of Thermal Spray Technology* 2(1): 21–29.

Oberdörster G (2001) Pulmonary effects of inhaled ultrafine particles. *International Archives of Occupational and Environmental Health* 74(1): 1–8. Available at:

http://www.springerlink.com/index/FVM951M11WWCV5JT.pdf%5Cnhttp://www.springerlink.com/openurl.asp?genre=article&id=doi:10.1007/s004200000185.

Occupational Safety and Health Admin. L (2006) 29 CFR 1910.134. Code of Federal Regulations, 427–451. Available at: https://www.osha.gov/pls/oshaweb/owadisp.show_document?p_table=standards&p_id=12716.

OJIMA J (2012) Gaseous Contaminant Distribution in the Breathing Zone. *Industrial Health* 50(3): 236–238. Available at: https://www.jstage.jst.go.jp/article/indhealth/50/3/50_MS1314/_article.

Pawlowski L (2008a) *The Science and Engineering of Thermal Spray Coatings*. *The Science and Engineering of Thermal Spray Coatings: Second Edition*. Available at: http://doi.wiley.com/10.1002/9780470754085.

Pawlowski L (2008b) *The Science and Engineering of Thermal Spray Coatings*. *The Science and Engineering of Thermal Spray Coatings: Second Edition*.

Petsas N, Kouzilos G, Papapanos G, Vardavoulias M and Moutsatsou A (2007) Worker Exposure Monitoring of Suspended Particles in a Thermal Spray Industry. *Journal of Thermal Spray Technology* 16(2): 214–219. Available at: http://link.springer.com/10.1007/s11666-007-9027-6.

Poland CA, Duffin R, Kinloch I, Maynard A, Wallace WAH, Seaton A, Stone V, Brown S, MacNee W and Donaldson K (2008) Carbon nanotubes introduced into the abdominal cavity of mice show asbestos-like pathogenicity in a pilot study. *Nature Nanotechnology*. Nature Publishing Group 3: 423. Available at: http://dx.doi.org/10.1038/nnano.2008.111.

Pope C and Dockery DW (2006) Health effects of fine particulate air pollution: Lines that connect. *Journal of the Air and Waste Management Association* 56(6): 709–742.

Pope C, RT B, MJ T and Al E (2002) Lung cancer, cardiopulmonary mortality, and long-term exposure to fine particulate air pollution. *JAMA* 287(9): 1132–1141. Available at: http://dx.doi.org/10.1001/jama.287.9.1132.

Pope CA, Dockery DW and Schwartz J (1995) Review of Epidemiological Evidence of Health Effects of Particulate Air Pollution. *Inhalation Toxicology* 7(1): 1–18.

Reche C, Viana M, Karanasiou A, Cusack M, Alastuey A, Artiñano B, Revuelta MA, López-Mahía P, Blanco-Heras G, Rodríguez S, Sánchez de la Campa AM, Fernández-Camacho R, González-Castanedo Y, Mantilla E, Tang YS and Querol X (2015) Urban NH3levels and sources in six major Spanish cities. *Chemosphere*. Elsevier Ltd 119: 769–777. Available at: http://dx.doi.org/10.1016/j.chemosphere.2014.07.097.

Salmatonidis A, Viana M, Pérez N, Alastuey A, de la Fuente GF, Angurel LA, Sanfélix V and Monfort E (2018) Nanoparticle formation and emission during laser ablation of ceramic tiles. *Journal of Aerosol Science*. Elsevier Ltd 126(September): 152–168. Available at: https://linkinghub.elsevier.com/retrieve/pii/S0021850218301897.

Schmid O and Stoeger T (2017) Surface area is the biologically most effective dose metric for acute nanoparticle toxicity in the lung. *Journal of Aerosol Science*. Elsevier 113: 276. Available at: http://dx.doi.org/10.1016/j.jaerosci.2015.12.006.

Seaton A, Tran L, Aitken R and Donaldson K (2010) Nanoparticles, human health hazard and regulation. *Journal of The Royal Society Interface* 7(Suppl_1): S119–S129. Available at: http://rsif.royalsocietypublishing.org/cgi/doi/10.1098/rsif.2009.0252.focus.

Shaffer RE and Rengasamy S (2009) Respiratory protection against airborne nanoparticles: A review. *Journal of Nanoparticle Research* 11(7): 1661–1672.

Strangman TE (1985) Thermal barrier coatings for turbine airfoils. *Thin Solid Films* 127(1–2):

93–106.

Tan JC, Looney L and Hashmi MSJ (1999) Component repair using HVOF thermal spraying. *Journal of Materials Processing Technology* 92–93: 203–208.

Toma FL, Stahr CC, Berger LM, Saaro S, Herrmann M, Deska D and Michael G (2010) Corrosion resistance of APS- and HVOF-sprayed coatings in the Al2O3-TiO2system. *Journal of Thermal Spray Technology* 19(1–2): 137–147.

Viana M, Fonseca AS, Querol X, López-Lilao A, Carpio P, Salmatonidis A and Monfort E (2017) Workplace exposure and release of ultrafine particles during atmospheric plasma spraying in the ceramic industry. *Science of the Total Environment* 599–600: 2065–2073.

Viitanen AK, Uuksulainen S, Koivisto AJ, Hämeri K and Kauppinen T (2017) Workplace measurements of ultrafine particles-A literature review. *Annals of Work Exposures and Health* 61(7): 749–758.

Voliotis A, Bezantakos S, Giamarelou M, Valenti M, Kumar P and Biskos G (2014) Nanoparticle emissions from traditional pottery manufacturing. *Environ. Sci.: Processes Impacts* 16(6): 1489–1494. Available at: http://xlink.rsc.org/?DOI=C3EM00709J.

WHO WHO (2017) *WHO Guidelines on Protecting Workers from Potential Risks of Manufactured Nanomaterials*. World Health Organization.

Table 1. Operational characteristics of each of the spraying booths and locations in the thermal spraying facility. N.A.: not available. APS: Atmospheric Plasma Spraying. HVOF: High Velocity Oxy-Fuel coating spraying.

Characteristics	**Booth #1**	**Booth #2**	**Booth #3**	**Central area**
Thermal spraying technique	APS	HVOF	HVOF	None
Spraying duration	20-30 minutes	5-10 minutes	5-10 minutes	None
Nr. repetitions/half-day	3	2	7-9	None
Type of parts coated	Large, single part	Large, single part	Small, several parts	None
Door	Mostly closed	Open	Open/closed	None
Volume (ca.,m^3)	84	114	68	465
Local exhaust/ventilation flow	N.A.	N.A.	6500 m^3/h	3×11800 m^3/h
Personal protective equipment				

Respirators	Pressurised respirator hood, FPP3 mask	FPP3 mask	FPP3 mask	None
Cloths	Protective jacket	None	Protective jacket	None
Gloves	High temperature gloves	None	High temperature gloves	None

Table 2. Mean particle number (N), particle diameter (Dp), lung deposition surface area (LDSA) from DiSCmini and mass (PM_1) concentrations during each of the activity periods monitored. Each half-day is labelled as (M) morning, (A) afternoon, or (cs) case study. N.A.: data not available. Statistical values: mean, standard deviation (SD), maximum (Max), minimum (Min) of each process calculated from non-normalized values for the total activity duration monitored during our studies (24-28/04/2017; DiSCmini).

		Near field (inside booths)				**Far field (worker area)**				**Inactivity**			
Date	**Feedstock**	**N (cm^{-3})**	**D_P (nm)**	**LDSA ($\mu m^2/cm^3$)**	**PM_1 ($\mu g/m^3$)**	**N (cm^{-3})**	**D_P (nm)**	**LDSA ($\mu m^2/cm^3$)**	**PM_1 ($\mu g/m^3$)**	**N (cm^{-3})**	**D_P (nm)**	**LDSA ($\mu m^2/cm^3$)**	**PM_1 ($\mu g/m^3$)**
Booth #1													
27/04 – M	Cr/Ni,	2.0×10^6	31.5	4.0×10^3	5.3×10^1	N.A.	N.A.	N.A.	N.A.	2.3×10^4	51.6	6.6×10^1	2.8×10^1
27/04 – A	Al_2O_3/TiO_2	1.6×10^6	36.8	3.1×10^3	6.9×10^1	5.8×10^4	40.0	1.2×10^2	4.4×10^1				
Mean		*1.8×10^6*	*34.2*	*3.6×10^3*	*6.1×10^1*	*5.8×10^4*	*40.0*	*1.2×10^2*	*4.4×10^1*	*2.3×10^4*	*51.6*	*6.6×10^1*	*2.8×10^1*

SD		*2.0×10^{5}*	*2.6*	*4.3×10^{2}*	*8.0×10^{0}*	*1.7×10^{4}*	*2.9*	*2.8×10^{1}*	*6.6×10^{0}*	*4.4×10^{3}*	*1.4*	*1.4×10^{1}*	*8.2×10^{0}*
Max		2.8×10^{6}	63.7	5.1×10^{3}	2.6×10^{2}	1.1×10^{5}	49.1	2.0×10^{2}	6.4×10^{1}	3.5×10^{4}	53.4	1.0×10^{2}	4.8×10^{1}
Min		5.2×10^{4}	12.1	4.6×10^{2}	3.0×10^{1}	3.4×10^{4}	33.2	8.5×10^{1}	3.2×10^{1}	1.7×10^{4}	49.2	4.9×10^{1}	1.9×10^{1}
Booth #2													
24/04 – A	WC/Cr/Co/Ni	3.4×10^{6}	37.2	5.8×10^{3}	1.7×10^{2}	3.5×10^{4}	75.6	1.5×10^{2}	N.A.	7.0×10^{3}	86.1	4.0×10^{1}	2.0×10^{1}
25/04 – M	WC/Cr/Co/Ni	5.3×10^{6}	28.3	7.6×10^{3}	1.0×10^{2}	5.4×10^{4}	54.3	1.7×10^{2}	8.3×10^{1}	6.3×10^{3}	123.3	4.9×10^{1}	2.9×10^{1}
26/04 – M	WC/Cr/Co/Ni	6.0×10^{5}	55.7	1.9×10^{3}	3.8×10^{1}	N.A.	N.A.	N.A.	N.A.	3.7×10^{4}	56.8	6.7×10^{1}	2.9×10^{1}
27/04 – cs	WC/Cr/Co/Ni	1.6×10^{6}	42.3	3.4×10^{3}	1.1×10^{2}	1.2×10^{5}	61.6	3.0×10^{2}	9.3×10^{1}	2.3×10^{4}	51.6	6.6×10^{1}	2.8×10^{1}
Mean		*2.7×10^{6}*	*40.9*	*4.7×10^{3}*	*1.0×10^{2}*	*6.9×10^{4}*	*63.8*	*2.1×10^{2}*	*6.5×10^{1}*	*1.8×10^{4}*	*79.5*	*5.6×10^{1}*	*2.5×10^{1}*
SD		*1.8×10^{6}*	*9.9*	*2.2×10^{3}*	*4.7×10^{1}*	*3.5×10^{4}*	*8.8*	*6.6×10^{1}*	*3.2×10^{1}*	*1.3×10^{4}*	*28.5*	*1.1×10^{1}*	*3.9×10^{0}*
Max		6.3×10^{6}	72.7	8.9×10^{3}	1.8×10^{3}	3.1×10^{5}	107.8	6.2×10^{2}	1.6×10^{2}	3.1×10^{5}	141.6	3.0×10^{2}	4.8×10^{1}
Min		7.6×10^{4}	19.8	2.1×10^{2}	3.3×10^{1}	9.3×10^{3}	45.7	4.3×10^{1}	4.1×10^{1}	2.8×10^{3}	50.5	2.1×10^{1}	1.9×10^{1}
Booth #3													
26/04 – M	WC/CrC/Ni	3.8×10^{6}	28.6	5.7×10^{3}	7.0×10^{2}	3.6×10^{5}	33.2	5.6×10^{2}	1.0×10^{2}	3.0×10^{4}	57.5	1.1×10^{2}	2.9×10^{1}
26/04 – A	WC/CrC/Ni	3.8×10^{6}	30.2	6.1×10^{3}	7.4×10^{2}	1.1×10^{5}	36.6	2.1×10^{2}	6.3×10^{1}				
28/04 – M	WC/CrC/Ni	3.1×10^{6}	31.3	5.1×10^{3}	5.2×10^{2}	1.7×10^{5}	46.4	3.9×10^{2}	1.0×10^{2}	5.8×10^{4}	33.9	1.0×10^{2}	2.4×10^{1}
28/04 – A	WC/CrC/Ni	2.9×10^{6}	32.1	4.8×10^{3}	5.8×10^{2}	1.5×10^{5}	42.1	3.2×10^{2}	8.4×10^{1}				
Mean		*3.4×10^{6}*	*30.6*	*5.4×10^{3}*	*6.4×10^{2}*	*2.0×10^{5}*	*39.6*	*3.7×10^{2}*	*8.7×10^{1}*	*4.4×10^{4}*	*45.7*	*1.1×10^{2}*	*2.7×10^{1}*
SD		*4.1×10^{5}*	*1.3*	*5.0×10^{2}*	*8.7×10^{1}*	*9.3×10^{4}*	*5.1*	*1.3×10^{2}*	*1.6×10^{1}*	*1.4×10^{4}*	*11.8*	*5.1×10^{0}*	*2.6×10^{0}*
Max		6.3×10^{6}	52.3	8.9×10^{3}	1.3×10^{3}	1.7×10^{6}	69.4	2.1×10^{3}	2.7×10^{2}	7.8×10^{4}	60.4	3.0×10^{2}	4.5×10^{1}

Min	1.9×10^{5}	10.0	2.2×10^{2}	2.1×10^{1}	3.3×10^{4}	18.4	8.6×10^{1}	1.8×10^{1}	1.5×10^{4}	29.4	5.0×10^{1}	2.0×10^{1}

Table 3. Dose rates in particle number($\dot{n}$), surface area ($\dot{s}$), mass ($\dot{m}$),and regional deposition to head airways, trachea bronchi and alveolar regions, calculated based on particle size-resolved concentration data (measured with NanoScan combined with MiniWRAS).

Dose rates	26/04/2017-Booth #3			28/04/2017- Booth #3		
	Inactivity	Morning	Afternoon	Inactivity	Morning	Afternoon
Mean Size (nm)	76	47	49	51	57	54
Total: $\dot{n}_{,}.10^{6}$ [min $^{-1}$]	138	1024	353	374	535	483
Head airways: $\dot{n}_{,}.10^{6}$ [min $^{-1}$]	16.3	163	61.7	40.2	106	91.3
Trachea bronchi: $\dot{n}_{,}.10^{6}$ [min $^{-1}$]	20.2	130	43.3	65.7	61.6	56.8
Alveolar: $\dot{n}_{,}.10^{6}$ [min $^{-1}$]	102	730	248	268	367	335
Total: $\dot{s}_{,}.10^{6}$ [μm^{2} min $^{-1}$]	1.8	6.3	3	1.8	5.7	4.4
Head airways: $\dot{s}_{,}.10^{6}$ [μm^{2} min $^{-1}$]	0.3	2	1.1	0.2	2.2	1.6
Trachea bronchi: $\dot{s}_{,}.10^{6}$ [μm^{2} min $^{-1}$]	0.2	0.54	0.3	0.3	0.4	0.3
Alveolar: $\dot{s}_{,}.10^{6}$ [μm^{2} min $^{-1}$]	1.2	3.8	1.7	1.3	3.1	2.5
Total I $\dot{m}_{,}$. [ng min $^{-1}$] (inactivity ρ=1.5 g cm^{-3}; Process ρ = 4.3 g cm^{-3})	1	9.5	5.5	0.8	8.5	11.5
Head airways: $\dot{m}_{,}$ [ng min $^{-1}$]	0.9	8.8	5.1	0.7	7.7	11

Trachea bronchi: $\dot{m}$, [ng min $^{-1}$]	0.02	0.2	0.1	0.02	0.2	0.1
Alveolar: $\dot{m}$, [ng min $^{-1}$]	0.1	0.5	0.3	0.1	0.6	0.4

Supplementary Data

Workplace exposure to nanoparticles during thermal spraying of ceramic coatings

Salmatonidis A., Ribalta C., Sanfélix V., Bezantakos S., Biskos G., Vulpoi A., Simion S., Monfort E., Viana M.

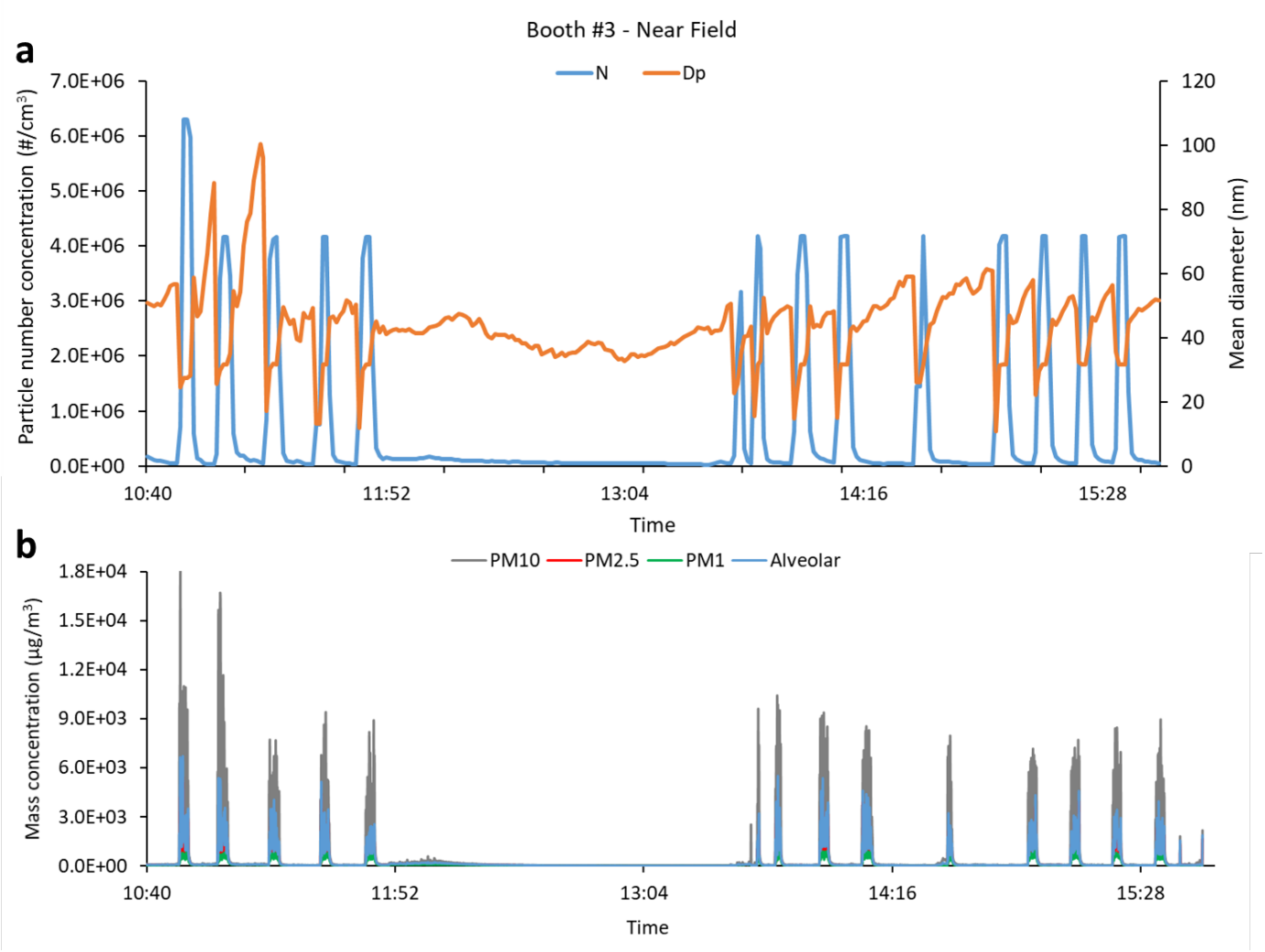

Figure S1. (a) Particle number concentration and mean diameter and (b) size segregated particle mass concentrations, in the near field location for booth #3 (28-04-2017).

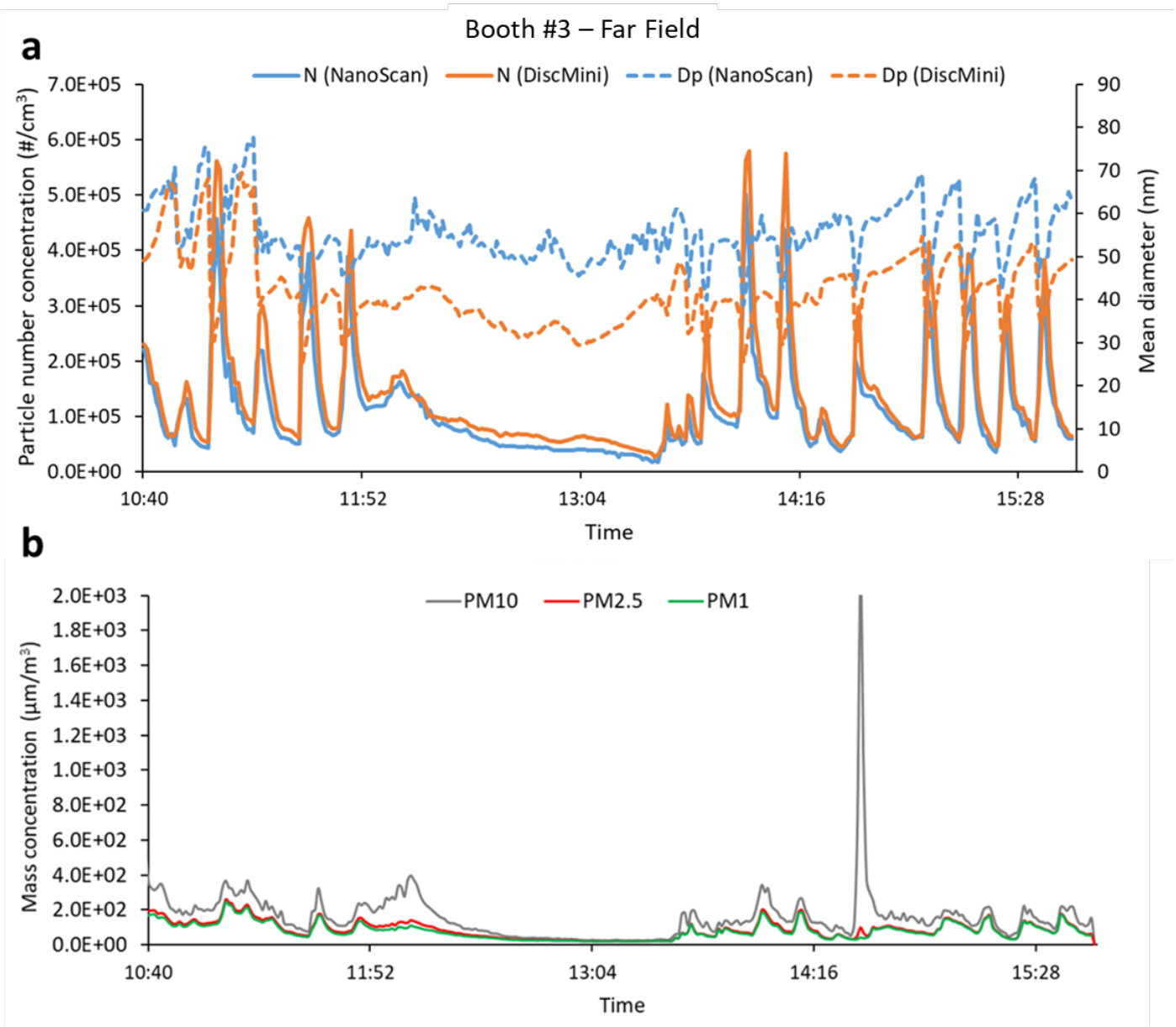

Figure S2. (a) Particle number concentration and mean diameter and (b) size segregated particle mass concentrations, in the far field location for booth #3 (28-04-2017)

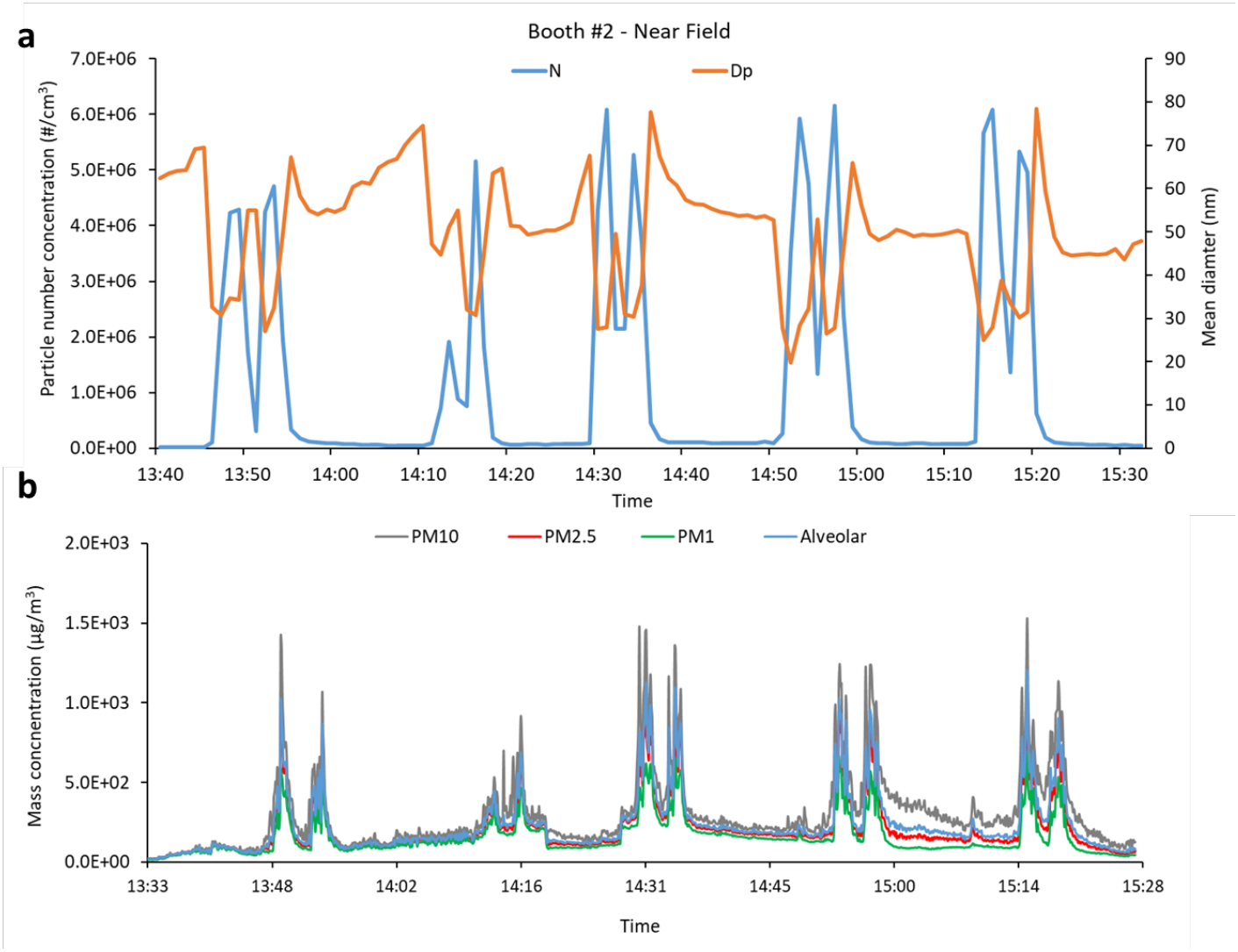

Figure S3 Particle number concentration and mean diameter and (b) size segregated particle mass concentrations, in the near field location for booth #2 (24-04-2017).

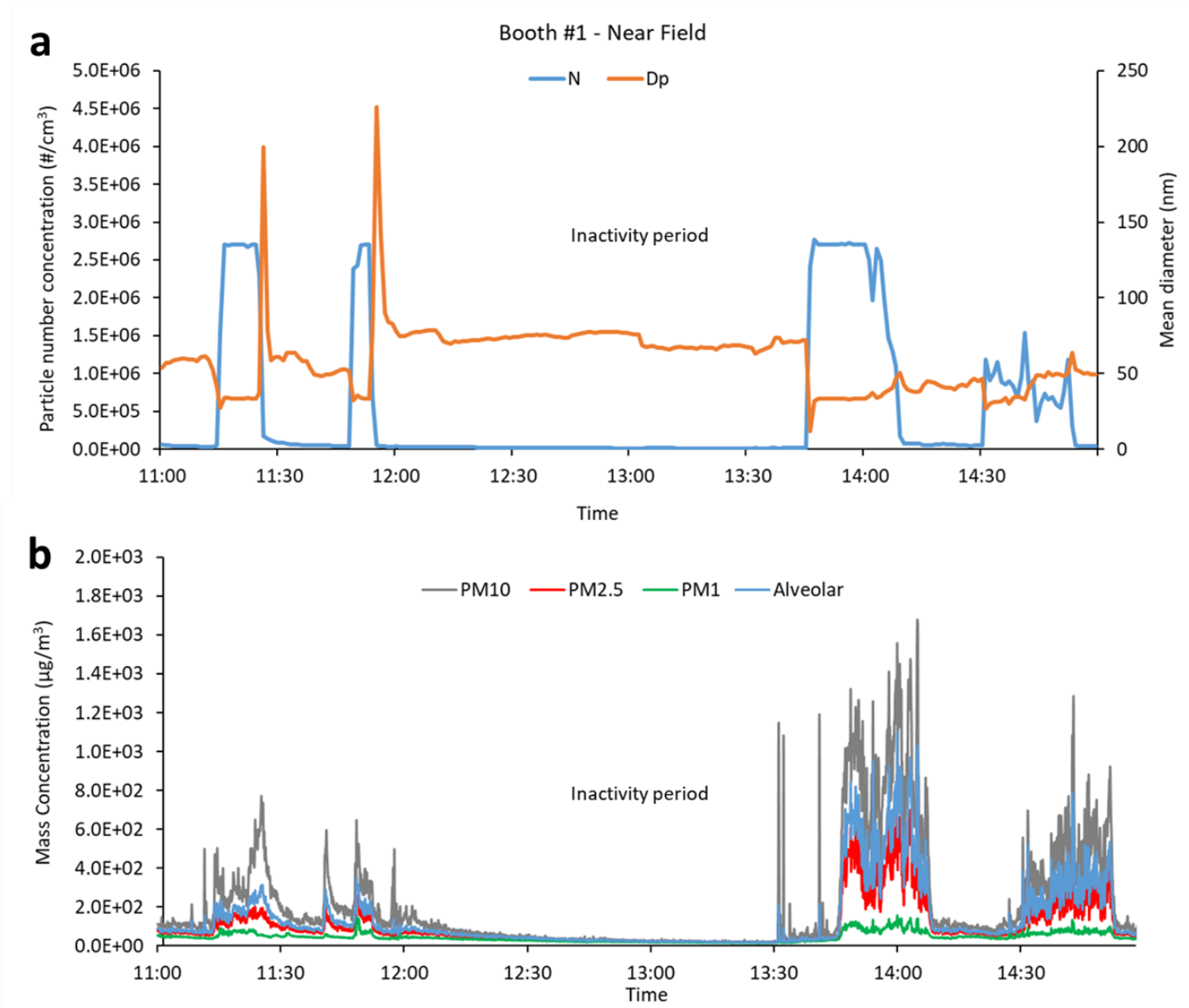

Figure S4 Particle number concentration and mean diameter and (b) size segregated particle mass concentrations, in the near field location for booth #1 (27-04-2017).

Table S1. Feedstock material characterisation. Material composition as provided by the manufacturer, and aggregate size measured by laser diffraction (Mastersizer-Malvern).

Booth	Feedstock	Material Composition (Blend)	Aggregate Size (µm)
Booth #1	ANVAL 50/50	Cr, Ni	76.5
Booth #1	Amdry 6228	TiO_2, Al_2O_3	36.0
Booth #2	Woka 3604	WC, Co, Cr, Ni	29.2
Booth #3	Woka 3702-1	WC, Cr_3C_2, Ni	34.3

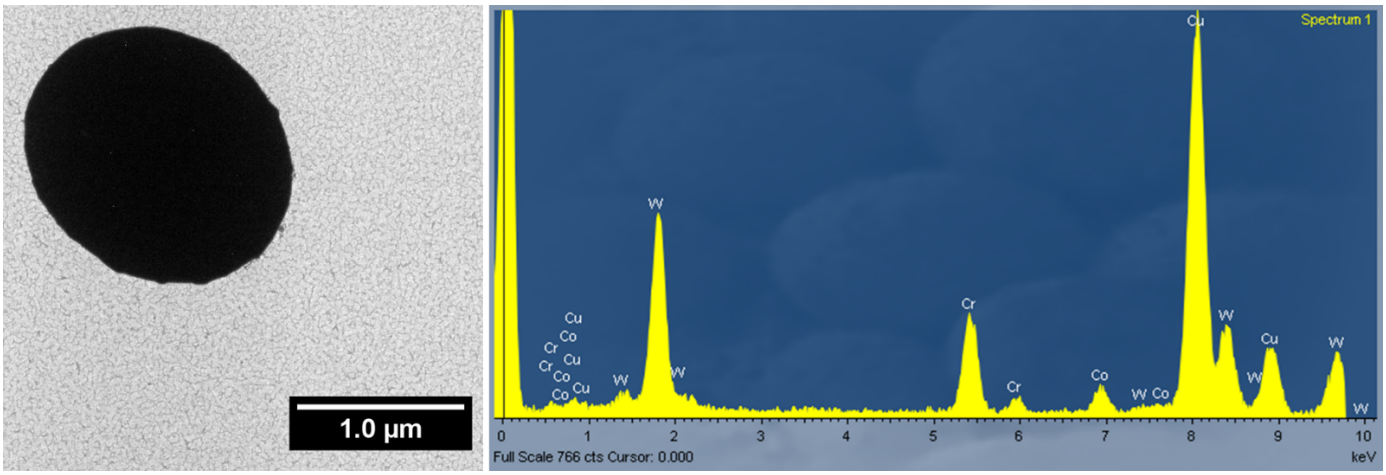

Figure S5. Particle > 1 µm emitted from Booth #3 (HVOF) having similar composition as the feedstock. Cu signal due to TEM grid.

Table S2. Instrument intercomparison results in terms of R^2 coefficients

Instrument	DiSCmini-UB	DiSCmini-ITC	DiSCmini-Impact	miniWRAS
DiSCmini-UB	-	$R^2 = 0.9978$	$R^2 = 0.9966$	-
DiSCmini-ITC	$R^2 = 0.9978$	-	$R^2 = 0.9981$	-
DiSCmini-Impact	$R^2 = 0.9966$	$R^2 = 0.9981$	-	-
CPC	$R^2 = 0.9461$	$R^2 = 0.9557$	$R^2 = 0.9503$	$R^2 = 0.8969$